Summer 8-15-2017

Nuclear export factor 3 regulates the localization of small nucleolar RNAs

Melissa Wanling Li
Washington University in St. Louis

WASHINGTON UNIVERSITY IN ST. LOUIS

Division of Biology and Biomedical Sciences

Molecular Cell Biology

Dissertation Examination Committee
Jean Schaffer, Chair
Thomas Baranski
Joseph Dougherty
Scot Matkovich
Jeanne Nerbonne
Joel Schilling

Nuclear export factor 3 regulates the localization of small nucleolar RNAs

By

Melissa Wanling Li

A dissertation presented to
The Graduate School
of Washington University in
partial fulfillment of the
requirements for the degree
of Doctor of Philosophy

August 2017

Saint Louis, Missouri

Table of Contents

List of Figures

CHAPTER TWO

CHAPTER THREE

CHAPTER FOUR

List of Tables

CHAPTER TWO

CHAPTER THREE

Acknowledgments

I would first like to thank my thesis mentor Dr. Jean Schaffer. Her relentless optimism and constant support have helped me accomplish things I did not think possible when I began my Ph.D. Her constructive criticism and attention to detail have not only made me a better experimentalist and science communicator, but has also built my self-esteem and confidence that I can accomplish anything. I would also like to thank the members of my thesis committee, Dr. Thomas Baranski, Dr. Joseph Dougherty, Dr. Scot Matkovich, Dr. Jeanne Nerbonne, and Dr. Joel Schilling for always challenging me to think critically and guiding me through my thesis these past six years. I would especially like to thank Dr. Scot Matkovich for his guidance and help with analyzing my RNA sequencing data.

I would not be here today without the support and collaboration of everyone in the Schaffer and Ory labs. I would like to thank Dr. Dan Ory for his willingness to answer my questions and provide input on my data. Words cannot express how grateful I am for the camaraderie of my fellow past and present graduate students: Dr. Aggie Bielska, Dr. Katrina Brandis, Dr. George Caputa, McKenna Feltes, Dr. Mia Henderson, Dr. Sarah Jinn, Dr. Maria Praggastis, Dr. Ben Scruggs, and Artie Sletten. Talking about experiments with them every day and getting their advice have been invaluable to me. Besides the day-to-day science discussions, they have all been my support system both inside and outside of lab. I will forever be grateful to Dr. Christopher Holley for his mentorship during my Ph.D. He was not just a role model in the lab but life in general. I

would like to thank Dr. Jiyeon Lee, Dr. Jamie Rimer, and Josh Langmade for their willingness to drop whatever they were doing to help anyone with an experiment or answer a question, no matter how small or big. I would also like to thank Sarah Gale whose positive attitude fueled the lab. The Schaffer and Ory labs would have a hard time functioning without you all. Even when science wasn't going well, these people made it worth it to continue to come into lab every day.

Thank you to all of the amazing friendships I have built during grad school. My friends have made me a better person and the support system they have provided me has been invaluable. I would not be who I am today without them. The times we have spent together are some of the best highlights of my life.

I would also like to thank my boyfriend Nick. I am so fortunate that we met early in grad school. Nick has listened to every complaint and every success I had in lab and his ability to make me laugh and feel loved has gotten me through all the ups and downs for the past six years. Thank you for being my constant reminder that life is good. My life wouldn't be the same without you.

Finally I would like to thank my family. My parents have sacrificed a lot to ensure I had every opportunity possible and words can never describe how thankful I am. I strive to be as thoughtful, generous and hard working as they are. They have always supported me and given me guidance in every aspect of my life. I would also like to thank my sister, Michelle. I am so fortunate to have a big sister who not only never hesitated to

give me advice, celebrate my successes with me, and always agreed to take jumping pictures with me, but she also has been my best friend through all stages of life. I am also grateful to my brother-in-law Jesse for his insightful advice and for truly being a brother to me. Their constant encouragement is why I am here today. Thank you for always pushing me to reach my full potential.

Melissa Wanling Li

Washington University in St. Louis

August 2017

Dedicated to my parents.

ABSTRACT OF DISSERTATION

Nuclear export factor 3 regulates the localization of small nucleolar RNAs

By

Melissa Wanling Li

Doctor of Philosophy in Biology and Biomedical Sciences

Molecular Cell Biology

Washington University in St. Louis, 2017

Professor Jean E. Schaffer, Chairperson

Metabolic diseases, such as obesity and diabetes, are associated with excess levels of lipids, which can lead to organelle dysfunction, cell death and eventually organ dysfunction. This process, termed lipotoxicity, is still not completely understood. In a genetic screen used to identify genes critical for lipotoxicity, the Schaffer lab has identified small nucleolar RNAs (snoRNAs) within the ribosomal protein L13a (*Rpl13a*) locus that mediate the cellular response to lipotoxic and general metabolic stress. These snoRNAs are non-canonical in that they accumulate in the cytosol after metabolic stresses like lipotoxicity and oxidative stress, suggesting that cells have specific mechanisms for regulating snoRNA distribution within the cell.

To begin elucidating the underlying mechanism of snoRNA transport from the nucleus to the cytoplasm during metabolic stress, we modeled oxidative stress by treating cells with the chemotherapeutic drug doxorubicin (DOX). DOX is a potent inducer of superoxide through the activation of NADPH oxidase splice isoform 4D (NOX4D) and results in the cytosolic accumulation of *Rpl13a* snoRNAs. NOX inhibitors and genetic

knockdown of NOX4D led to a decrease in the accumulation of *Rpl13a* snoRNAs in the cytosol after DOX treatment. Furthermore, RNA-sequencing studies demonstrated that snoRNAs as a class accumulated in the cytosol after DOX treatment, while simultaneous treatment with NOX inhibitors blunted the increase in cytosolic levels of snoRNAs. Together, these data indicate that snoRNAs as a class are present in the cytoplasm, where their levels are dynamically regulated by NOX4D during oxidative stress.

The finding that loss-of-function of NXF3, a member of the nuclear export family of RNA transporters, protects cells from lipotoxic cell death suggested that this protein may function as a regulator of snoRNA distribution. In transient transfection assays, NXF3 knockdown increased abundance of cytosolic *Rpl13a* snoRNAs, whereas NXF3 overexpression led to decreased cytosolic levels. These observations suggested that snoRNAs traffic constitutively between the nucleus and cytoplasm, and NXF3 functions to efficiently concentrate snoRNAs in the nucleus. Consistent with a role for NXF3 as a snoRNA transporter, we found the *Rpl13a* snoRNAs co-immunoprecipitated with NXF3. Treatment of cells with forskolin caused a rapid decrease in cytosolic snoRNAs and increased both nuclear localization of NXF3 and association of NXF3 with *Rpl13a* snoRNAs. These effects of forskolin were abrogated by NXF3 knockdown.

Our findings identify a novel trafficking pathway for snoRNAs that cycle between the nucleus and the cytosol. This pathway is regulated by oxidative stress and levels of the RNA transporter NXF3.

CHAPTER ONE:
Introduction

1.1 Obesity and diabetes are global health concerns

Obesity is a major risk factor for metabolic diseases such as diabetes, and both have become increasingly prevalent worldwide. Obesity has more than doubled since 1980. In 2014, more than 1.9 billion adults were overweight, 600 million of whom were obese and 422 million of whom were diagnosed with diabetes (WHO Diabetes fact sheet, 2016). These diseases have been attributed to accelerated urbanization, increased caloric intake, changes in types of caloric intake, and sedentary lifestyles (WHO Diabetes fact sheet, 2016; Globalization of Diabetes Hu, 2011).

Many complications can arise from obesity and diabetes, and these contribute to substantial morbidity and mortality. Cardiovascular disease accounts for 51% of deaths in patients with type 1 diabetes and 52% of deaths in patients with type 2 diabetes [1]. Diabetic heart diseases include coronary heart disease (CHD) and heart failure. CHD occurs when atherosclerotic plaque builds up inside coronary arteries, a condition that causes myocardial infarction. Although heart failure can result from the damage caused by infarcts, a clinically distinct form of heart failure called diabetic cardiomyopathy (DCM) is characterized by ventricular dilation, myocyte hypertrophy, interstitial fibrosis and decreased diastolic and/or systolic function that occurs in the absence of underlying atherosclerotic disease [2-4].

In addition to macrovascular complications, diabetic individuals have an increased prevalence in microvascular complications, such as diabetic retinopathy, which is the leading cause of blindness (NEI Diabetic Retinopathy, 2010), and diabetic neuropathy, which accounts for 60% of non-traumatic lower-limb amputations in American adults (CDC National Diabetes Statistics Report, 2014). Diabetes is also the primary cause of kidney failure accounting for 44% of new cases (CDC National Diabetes Statistics Report, 2014). In addition to vascular diseases, people with diabetes are also at a higher risk for some cancers [5].

Currently, obesity and diabetes are linked to more deaths worldwide than malnutrition (WHO Diabetes fact sheet, 2016). In 2016, 1.5 million deaths were directly caused by diabetes, which is the seventh leading cause of death overall (CDC At a Glance Fact Sheets 2016). Given the high prevalence of obesity and diabetes, the medical costs of treating the disease and its associated complications have become enormous. It is estimated that the cost of diabetes care in 2015 alone worldwide was $1.31 trillion USD [6]. A greater understanding the pathogenesis of this disease is essential to decrease morbidity and mortality and to reduce this growing socioeconomic burden worldwide.

1.2 Systemic metabolic abnormalities in diabetes

As the primary source of the body's energy, blood glucose levels are tightly regulated to keep the body in homeostasis. When blood glucose levels are low, pancreatic α-cells secrete glucagon that converts glycogen into glucose in order to raise blood glucose levels. Meanwhile, when glucose levels are high, pancreatic β-cells release insulin,

which signals to cells to take up glucose from blood through the GLUT4 transporter and to liver and muscle cells to store glucose as glycogen, both of which lower blood glucose levels. Inadequate insulin action and hyperglycemia is a hallmark of diabetes. In type 1 diabetes patients, the immune system destroys β-cells, preventing the pancreas from producing insulin. It is thought to arise from genetic factors and environmental triggers. However, type 1 diabetes accounts for only 5-10% of all diabetes cases [7]. By contrast, in type 2 diabetes, the pancreas produces insulin, but tissues in the body become resistant to the actions of the hormone. The inability of insulin to signal to tissues to take up blood glucose leads to hyperglycemia [8]. With obesity on the rise, type 2 diabetes cases have also increased, with the number of Americans diagnosed with diabetes increasing fourfold from 1980 through 2014 (5.5 million to 22.0 million) (CDC Diagnosed Diabetes, 2015). Prolonged exposure of hyperglycemia has been linked to the pathogenesis of complications in both type 1 and type 2 diabetes, including heart disease, retinopathy and glomerulopathy [9-11].

Large multicenter studies that have tested the ability of tight glycemic control for the prevention of complications have provided evidence for efficacy in preventing some, but not all diabetic complications. For example, the DCCT/EDIC trial demonstrated that tight glycemic control in patients with type 1 diabetes reduced the incidence and severity of macrovascular and microvascular disease [12]. However, in the ACCORD trial, treating hyperglycemia alone in type 2 diabetes was sufficient to decrease microvascular complications, but did not have a beneficial effect on macrovascular complications such as CHD [13]. These findings and similar observations in other studies of type 2 diabetes

suggested that other associated metabolic disturbances in diabetes may contribute importantly to complications. For example, in addition to hyperglycemia, patients with type 2 diabetes often have high circulating triglycerides and free fatty acids (FFA) [14-16]. Hypertriglyceridemia is linked to the incidence and severity of complications, including neuropathy, retinopathy, non-alcoholic steatohepatitis, heart failure [17-20].

1.3 Lipotoxicity

FFAs and their metabolites are crucial as an energy source, as components of cellular membranes, and as signaling molecules in many physiological processes. Besides exogenous sources of FFA in the diet, lipogenic tissues can generate lipids de novo from excess carbohydrates [21]. In conditions of nutritional excess, FFAs are metabolized to triacylglycerides (TAGs) and stored in neutral lipid droplets in adipose depots. During nutritional deprivation or sympathetic stimulation, TAGs are hydrolyzed into glycerol and FFAs, which are released into the bloodstream for distribution of this energy source to peripheral tissues. The liver also produces FFA and triglycerides, which are secreted into the circulation as lipoproteins. The hormone insulin negatively regulates lipolysis in adipose tissue and de novo lipogenesis in the liver. In the setting of insulin resistance, levels of lipids in the blood stream are high and can further contribute to insulin resistance in tissues such as skeletal muscle [22-24]. Hyperlipidemia may also reflect the finite capacity for expansion of adipose tissue stores of triglyceride in obesity.

Hyperlipidemia causes increased delivery of FFA and triglycerides to non-adipose tissues. These tissues have some capacity to metabolize or store FFA as triglyceride in

ectopic lipid droplets. Studies of cultured cells and animal models suggest that this initial storage of excess lipid as triglyceride is protective [25-28]. However, this capacity for triglyceride storage in non-adipose tissues is limited. Ultimately, FFA that fail to be sequestered in triglyceride droplets or that are released from TAG hydrolysis can lead to cell dysfunction and eventually cell death, a process termed lipotoxicity.

Hyperlipidemia also induces generation of reactive oxygen species (ROS). ROS are highly reactive molecules with an unpaired electron that are produced during normal cellular metabolism. One source of endogenous ROS is the electron transport chain (ETC) in the mitochondria. As electrons are shuttled through the ETC, incomplete one-electron reduction of oxygen can occur, generating superoxide (O_2^-), instead of reduction of oxygen to water. In addition, there are several enzymatic pathways that produce ROS [29]. For example, nicotinamide adenine dinucleotide phosphate oxidase (NOX) is an oligomeric protein that can generate O_2^- [30]. Besides the NOX family, other enzymes that produce ROS include myeloperoxidase, which is expressed in neutrophils and produces hypochlorous acid; xanthine-oxidase, which catalyzes the oxidation of xanthine or hypoxanthine into uric acid; and nitric oxide synthase, which synthesizes nitric oxide required for vascular tone, neurotransmission and inflammation [29]. Cells express several ROS scavenging enzymes, such as catalase and glutathione peroxidases, and proteins with redox active centers that protect against oxidative stress and enable cells to maintain ROS levels at relatively low levels during homeostatic conditions. Nonetheless, certain stresses, such as hyperlipidemia, trigger an increase in ROS production that exceeds the cell's antioxidant capacity. When this occurs, high

levels of ROS can damage DNA, post-translationally modify proteins in ways that alter their function, and lead to lipid peroxidation [29]. For example, excess free fatty acids, present in metabolic diseases such as type 2 diabetes, produce high levels of ROS through activation of NOX, through membrane remodeling, and through prolonged ER stress that ultimately lead to cell dysfunction and cell death [31-34].

The proper function of the endoplasmic reticulum (ER) is necessary for lipid and protein metabolism under homeostatic conditions. Mutant proteins disrupt protein folding in the ER, leading to a halt in protein translation, degradation of misfolded proteins, and activation of signal pathways that increase the production of chaperones involved in protein folding. If the ER stress is not resolved, this triggers the activation of pro-apoptotic genes and activation of NOX resulting in oxidative stress [35,36]. Lipids also cause ER stress. As the major site for synthesis of lipids that constitute biological membranes, the ER plays an important role in membrane lipid homeostasis. Treating cells with pathophysiological levels of saturated fatty acid palmitate, but not general oxidative stress-inducer H_2O_2, leads to a change in ER membrane composition, thus compromising ER structure and integrity [31]. The resulting ER and oxidative stress lead to cellular dysfunction and ultimately, cell death [31,37]. However similar concentrations of unsaturated long-chain FFAs are well tolerated. Studies have shown that co-treating cells with saturated and unsaturated long-chain FFAs rescues cells from lipotoxicity [31,38]. These observations have been linked to the greater capacity of cells to store unsaturated FFA as triglyceride and the ability of of unsaturated FFA to enhance palmitate incorporation into triglyceride stores [26].

On a systemic level, prolonged hyperlipidemia has been associated with dysfunction of many organs. In diabetes, non-alcoholic steatohepatitis [39], glomerulopathy [40], and cardiomyopathy [41] are associated with ectopic lipid accumulation in these non-adipose tissues. In patients with congenital lipodystrophies, diminished or absent adipose tissue leads to ineffective FFA storage and hyperlipidemia that is associated with profound non-alcoholic steatohepatitis and systemic insulin resistance [42]. Although strategies to decrease serum lipid levels through behaviorial interventions, such as exercise and improved diets, or by inhibiting de novo lipogenesis can be efficacious, strategies to prevent lipotoxicity are limited by our incomplete knowledge of the mechanisms underlying FFA-induced cellular injury.

1.4 *Rpl13a* snoRNAs mediate cellular response to metabolic and oxidative stresses

In order to identify novel regulators of the cellular response to lipid overload, the Schaffer lab has used a cell culture model of lipotoxicity in which non-adipose cells are grown in media supplemented with pathophysiological levels of the saturated fatty acid palmitate. Under these conditions, fibroblasts, hepatocytes, cardiomyoblasts, and endothelial cells develop ER and oxidative stress and ultimately die over the course of 24 to 48 hours. The Schaffer lab used this model to perform a loss-of-function genetic screen using the ROSABgeo promoter trap. The integrated ROSABgeo provirus contains B-galactosidase-neomycin phosphotransferase fusion cassette with a strong polyadenylation sequences, but lacks its own promoter. Therefore, the ROSABgeo

transcript is only expressed if it integrates downstream of an actively transcribed RNA polymerase II promoter. In this case, the neomycin phosphotransferase activity allows the mutant to survive neomycin selection, and because of the strong polyadenylation sequence, the endogenous gene at the site of the integration is no longer expressed. The genetic screen was performed in Chinese hamster ovary (CHO) cells, and mutants with single promoter trap integrations were selected for growth over 48 hours in the presence of lipotoxic levels of palmitate [31,43-46].

The locus encoding ribosomal protein L13a (*Rpl13a*) was identified as the site of mutation in one of these mutant cell lines and is necessary for the production of oxidative stress and cell death in response to lipotoxic stress [45]. The eight exons in this locus encode the *Rpl13a* protein, a constituent of the large ribosomal subunit. This locus also contains four intronic box C/D small nucleolar RNAs (snoRNAs)—U32a, U33, U34, and U35a—that are produced from the intron lariats generated during splicing of the *Rpl13a* pre-mRNA. Through complementation and directed knockdown experiments, the Schaffer lab showed that loss of the intronic *Rpl13a* snoRNAs, rather than the *Rpl13a* protein, were responsible for palmitate resistance in the mutant cell line. Furthermore, while the *Rpl13a* snoRNAs are enriched in the nucleus of wild type cells under basal conditions, they are also detected in the cytoplasm and they rapidly accumulate in the cytosol in response to lipotoxicity and general inducers of oxidative stress [44,45,47]. Another mutant isolated from the screen had a disruption in the SmD locus, a core component of the spliceosome that was shown to be necessary for the correct processing of snoRNAs from intron lariats [46]. Intriguingly, haploinsufficiency of

the *Rpl13a* snoRNAs is sufficient to confer protection from lipotoxicity, but does not alter the 2'-O-methylation of predicted rRNA targets [45]. Together, these experiments suggest a potential non-canonical role for the *Rpl13a* snoRNAs outside of the nucleus in the cellular response to metabolic stress.

1.5 Small nucleolar RNAs

The *Rpl13a* snoRNAs are members of a broader class of short noncoding RNAs that range from 60-200 nucleotides long. Most mammalian snoRNAs, including the *Rpl13a* snoRNAs, are encoded within introns, are processed out of intron lariats during splicing, and lack a 5' cap structure. There is a small subset of snoRNAs that are independently transcribed by RNA polymerase II that includes U3, U8 and U13, and in their mature form contain an m_3G cap [48]. SnoRNAs are categorized as belonging to the box C/D or box H/ACA class based on conserved sequence motifs. Both classes of snoRNAs complete their maturation to functional ribonucleoproteins (RNPs) with a core set of proteins in Cajal bodies and then localize within the nucleolus.

Most snoRNAs are known to function in the covalent modification of other noncoding RNAs within the nucleolus. Specifically, box C/D snoRNAs complex with the methyltransferase fibrillarin and guide 2'-O-methylation of ribosomal RNAs (rRNA), while box H/ACA snoRNAs complex with the pseudouridine synthase dyskerin and guide pseudouridylation of rRNAs. Both classes of snoRNAs contain short (10-20 nucleotides for box C/D snoRNAs) antisense elements that are complementary to the sequence of their target RNAs, and serve as zipcodes to target the mature snoRNPs to

bind specific sites of modification on the target RNAs. SnoRNAs that stay and function within the Cajal bodies are called small Cajal body-specific RNA (scaRNA). ScaRNAs guide 2'-O-methylation and pseudouridylation on small nuclear RNAs (snRNA) [49]. A number of snoRNAs are considered orphans on the basis that there is no known target rRNA [50]. In some instances, snoRNA-directed modifications have been shown to be necessary for proper ribosome and spliceosome function [51-54], for processing of pre-rRNA species [55], or for stability of rRNA [56]. In addition, there is a growing body of evidence of snoRNA roles outside of rRNA or snRNA modification, including roles in modification of pre-mRNAs to direct splicing [57], regulation of RNA editing [58], miRNA-like post-transcriptional regulation [59], and pseudouridylation of mRNA targets [60].

Recent studies also provide evidence for novel functions of snoRNAs in disease states. In a knock-in mouse model with loss-of-function of the *Rpl13a* snoRNAs generated by the Schaffer lab, cells and tissues from the knock-in mouse have lower basal ROS tone and are resistant to metabolic stress and diabetogenic stimuli [61]. This suggests that *Rpl13a* snoRNAs could play a role in metabolic diseases. SnoRNAs have also been implicated in cancer. Box C/D snoRNA U50 is downregulated in prostate cancer and breast cancer [62], while box H/ACA snoRNA SNORA42 is overexpressed in non-small-cell lung cancer [63]. Furthermore, deletions that included loss of box C/D snoRNAs SNORD14D, SNORD43, U34 and U35a, suppressed leukaemogenesis [64]. Together, these findings implicate snoRNAs in disease pathogenesis.

The finding that *Rpl13a* snoRNAs are present in the cytosol under homeostatic conditions and the observation that metabolic stress conditions regulate the cytosolic levels of these and other snoRNAs suggests these non-coding RNAs could have functions outside the nucleus. Since knockdown and loss-of function approaches to study the functions of snoRNAs affect the nuclear and cytosolic pools of the targeted species, these approaches have limited ability to identify roles of snoRNAs in specific subcellular compartments. In order to elucidate potential functions of snoRNAs in the cytosol, it would be ideal to disrupt trafficking of these non-coding RNAs out of the nucleus. However, mechanisms that regulate movement of snoRNAs between the nucleus and cytoplasm are poorly characterized. In the present study, we demonstrate that the dynamic localization of snoRNAs is regulated by superoxide through DOX-induced activation of enzyme NOX4D.

1.6 RNA transporters

Most RNAs exit the nucleus complexed as RNPs through the nuclear pore complexes (NPC) that are made up of nucleoporin proteins. Members of the nuclear export factor (NXF) family play important roles in the export of RNA by physically interacting with the nucleoporins to facilitate export. The NXF family is comprised of five functional members NXF1, NXF2, NXF3, NXF5 and NXF7. NXF family members have been identified based on similarity of sequence and domain architecture. Most include an amino terminal RNA binding interaction domain, a p15/NXFt-heterodimerization domain that recruits NXF adaptor p15 necessary for nuclear transport, and a carboxyl terminal ubiquitin associated domain involved in NPC binding [65,66].

NXF family members have been shown to function in the transport of specific classes of RNAs. For example, Nuclear export factor 1 (NXF1) is considered the bulk mRNA transporter. NXF1 operates with several other proteins, including ALY and a cap-binding complex, which help target its mRNA cargo, and with p15, which helps the NXF1-mRNA complex physically interact with nucleoporins to exit the nucleus through the NPC. Unlike other RNA transport, NXF1-mediated mRNA export is RanGTP independent indicating that directionality of transport is established through a different mechanism [67]. NXF2, NXF3 and NXF5 have also been shown to function in the nuclear export of mRNAs, whereas NXF7 has been proposed to function in the cytoplasmic trafficking of mRNAs [68-73].

Other classes of transporters have been shown to be involved in nucleocytoplasmic transport of small RNA species. The transport of tRNAs is mediated through exportin-t and transport of miRNAs is mediated through exportin-5. Both exportins directly bind their target RNA in an RanGTP-dependent manner. The exportin-RNA-RanGTP complex is exported through the NPC to the cytoplasm where RanGTP is hydrolyzed, thus releasing its cargo in the cytoplasm. Export receptor CRM1 is required for snRNA export and is also RanGTP-dependent. However, unlike tRNA and miRNA export, in which their specific export receptors bind directly to their target RNA, CRM1 requires adaptor protein PHAX and a cap binding complex to bind to its RNA cargo [67].

SnoRNAs have long been thought to complete their biogenesis and function within the nucleus. In eukaryotic cells, most snoRNAs are encoded within pre-mRNA introns, while some snoRNAs are independently transcribed. Both types of snoRNAs are transcribed in the nucleus. SnoRNP proteins, like fibrillarin and dyskerin, bind immature pre-snoRNAs while they are trimmed by exonucleases in the nucleoplasm. The snoRNPs are then trafficked to the Cajal bodies for maturation. Mature snoRNPs either stay within the Cajal body, as is the case for scaRNAs, or traffic to the nucleolus where they guide the modification of newly synthesized rRNAs [51,54,74]. Nuclear export receptors PHAX and CRM1 are necessary to sequentially transport independently-transcribed snoRNA U3 from the Cajal body to the nucleolus for correct snoRNP maturation [75]. Although PHAX and CRM1 can also function as export receptors, there is not evidence that they are involved in nucleocytoplasmic transport of U3 or other snoRNAs.

Nonetheless, several studies suggest that cells have endogenous mechanisms for transport of independently transcribed and capped snoRNAs between the nucleus and cytoplasm. Xenopus oocytes provide evidence for an endogenous pathway that transports capped U3 from the cytoplasm to the nucleus following microinjection of in vitro transcribed U3 [75]. Moreover, U8 snoRNA associates with the import factor snurportin 1 in mammalian cells, and knockdown of this transport adaptor is associated with increased cytosolic U8 [76]. Whether snurportin 1 serves a broader role in transport of the overall class of snoRNAs, and whether other transport proteins function to regulate the distribution of snoRNAs between the nucleus and cytoplasm is not known. In particular, it is uncertain whether these mechanisms apply to intronic, uncapped

snoRNA transport. In the present study, we identified nuclear export factor (NXF3) as a snoRNA nucleocytoplasmic transporter that can be regulated by cyclic AMP and ROS levels.

CHAPTER TWO:
Metabolic stress regulates snoRNA trafficking

2.1 INTRODUCTION

The four intronic box C/D snoRNAs from the *Rpl13a* locus are critical mediators of lipotoxicity [45]. Although snoRNAs are thought to reside and function exclusively in the nucleolus, the *Rpl13a* snoRNAs rapidly accumulate in the cytosol when cells are exposed to pathophysiological levels of palmitate, a known inducer of oxidative stress. In addition, oxidative stress resulting from hydrogen peroxide treatment also causes these snoRNAs to accumulate in the cytosol [44,45]. These observations suggested that ROS is an important regulator of snoRNA localization.

Reactive oxygen species (ROS) are highly reactive molecules with unpaired electrons that are produced during normal cellular metabolism. A major source of endogenous ROS is the electron transport chain in the mitochondria [77]. In addition, there are several enzymatic pathways that produce ROS [78]. Nicotinamide adenine dinucleotide phosphate oxidase (NOX) is an oligomeric protein that can generate superoxide. There are seven isoforms of the NOX catalytic subunit, each characterized by a cytoplasmic N-terminus, six transmembrane domains, and a long cytosolic C-terminal tail. All seven isoforms, except for NOX5, require the transmembrane protein $p22^{phox}$ for stability and activation [30,79]. However, the isoforms differ with respect to tissue distribution and subcellular localization. NOX2 is considered the prototype NOX. It is localized in the membranes of phagosomes and highly expressed in phagocyte-specific tissues, where

its ROS production contributes to the elimination of microbes [30]. On the other hand, NOX4 is known to localize in the mitochondria in the heart, where it is constitutively active [30,80]. There are four splice variants of NOX4 (NOX4B, NOX4C, NOX4D and NOX4E) that may have different functions in ROS-related signaling. Specifically, splice variant NOX4D lacks the transmembrane domain and is found to localize within the nucleus [81,82], raising the possibility that it could be involved in generating ROS in the vicinity of snoRNAs.

Although snoRNAs have been established as guides to 2'-O-methylation and pseudouridylation of other small noncoding RNAs within the nucleus, their role in the cytosol and regulation of their localization outside of the nucleus have previously not been investigated. Our goal was to investigate the mechanisms underlying the cytosolic localization of *Rpl13a* snoRNAs under metabolic stress conditions and to determine whether the cytosolic localization applies specifically to the *Rpl13a* snoRNAs or to the snoRNAs as a class.

2.2 RESULTS

2.2.1 Doxorubicin treatment increases cytosolic *Rpl13a* snoRNA levels in cardiomyoblasts

Our lab has previously demonstrated that the accumulation of cytosolic *Rpl13a* snoRNAs begin to accumulate in the cytosol after treatment with 6-8 h of palmitate or 3-5 h of hydrogen peroxide, both of which induce high levels of cellular ROS [44,45]. Another potent inducer of ROS is the chemotherapy drug doxouribicin (DOX) [83,84]. We treated

H9c2 rat cardiomyoblasts with 20 μM DOX for 1 h, isolated the cytosolic and nuclear fraction of cells using sequential detergent extraction, and used RT-qPCR to measure levels of the *Rpl13a* snoRNAs relative to Rplp0. As expected, prior to DOX treatment, U32a, U33 and U34 levels were 400-500X more abundant in the nuclear fraction than the cytosolic fraction (**Figure 2.1A**). Cytosolic proteins (HSP90, α-tubulin) were enriched in the cytosolic fraction while nuclear proteins (nucleophosmin and histone H3) were enriched in the nuclear fraction (**Figure 2.1B**). After DOX treatment, we detected 12-, 4-, and 8-fold increases in the cytosolic abundance of U32a, U33, and U34 (**Figure 2.1A**). The levels of total and nuclear *Rpl13a* snoRNAs were not significantly increased after DOX treatment and the nuclear proteins did not appear in the cytosolic fraction after DOX treatment. This suggests that the observed increase in the *Rpl13a* snoRNAs is not due to any decrease in nuclear integrity or overall increase in total snoRNA levels (**Figure 2.1A-C**).

2.2.2 Superoxide is necessary for cytosolic *Rpl13a* snoRNA accumulation during doxorubicin treatment

DOX has been shown to induce superoxide through the NOX enzymes [85,86]. To determine whether the localization of the *Rpl13a* snoRNAs during DOX treatment was dependent on superoxide, we tested whether NOX inhibitor DPI or the superoxide scavenger Mn(III)TMPyP (MnT) could inhibit the cytosolic accumulation of the *Rpl13a* snoRNAs. Co-treatment of H9c2 rat cardiomyoblasts with DPI or MnT, blunted the DOX-induced accumulation of cytosolic *Rpl13a* snoRNAs (**Figure 2.2A**). Moreover, treating H9c2 rat cardiomyoblasts with DPI alone resulted in lower levels of cytosolic

snoRNAs (**Figure 2.2B**). Together, these results suggest the production of superoxide by a NOX enzyme is required for *Rpl13a* snoRNA accumulation in the cytosol both after DOX treatment and under normal homeostatic conditions. We next tested whether the inhibitory effects of DPI and MnT on cytosolic snoRNA accumulation simply reflected inhibition of DOX-induced nucleolar stress. We performed immunofluorescence staining of the nucleolar protein nucleophosmin (NPM) to assess nucelolar integrity during DPI, MnT and DOX treatments [87]. Nucleolar punctae, present under basal conditions, were lost after DOX treatment, consistent with nucleolar stress, but NPM staining remained localized within the nucleus (**Figure 2.2C**). Thus, although MnT and DPI blunted the accumulation of cytosolic *Rpl13a* snoRNAs after DOX treatment, the drugs had no effect on the DOX-induced nucleolar stress, suggesting that the nucleolar dissolution is not dependent on superoxide or NOX activity. Together, our results are consistent with a model in which *Rpl13a* snoRNA accumulation in the cytosol is dependent on ROS and is not the result of generalized nucleolar stress.

2.2.3 NADPH oxidase 4D mediates cytosolic *Rpl13a* snoRNA accumulation in response to doxorubicin treatment

The ability of DPI and MnT to inhibit cytosolic snoRNA accumulation after DOX suggested a mechanism involving the NOX enzyme family. In cardiomyoblasts, NOX4 activity is dependent on the p22 subunit, and one of its four splice variants, NOX4D, localizes in the nucleus and nucleolus [82,88]. Given its localization, we hypothesized that NOX4D could generate nuclear ROS to impact snoRNA localization. Given the gene structure of NOX4D, it was not possible to design an siRNA specific to NOX4D (**Figure**

2.3). We used two independent siRNAs against the following targets: NOX4A at exons 3 or 5 (siRNA NOX4A), both NOX4A and NOX4D isoforms at exons 12-13 or 14 (siRNA NOX4AD), or the regulatory p22 subunit. Following transfection of cardiomyoblasts, total mRNA levels of p22 were significantly knocked down by two independent siRNAs (**Figure 2.4A**). Total mRNA levels of NOX4A were significantly knocked down by all NOX4A and NOX4AD siRNAs (**Figure 2.4B**). Total mRNA levels of NOX4D were significantly knocked down only by NOX4AD siRNAs (**Figure 2.4C**). Knockdown of these targets was not affected by DOX treatment (**Figures 2.4A-C**). SiRNA against NOX4AD and p22 recapitulated the effects of MnT and DPI, significantly blunting cytosolic accumulation of *Rpl13a* snoRNAs after DOX treatment, whereas siRNA against NOX4A only had no significant effect (**Figures 2.4D**). These data implicate NOX4D as a mediator of cytosolic snoRNA accumulation in response to DOX treatment. Similar to DPI and MnT treatment, none of the siRNA knockdowns inhibited nucleolar stress induced by DOX (**Figure 2.4E**).

2.2.4 SnoRNAs are dynamically regulated in the cytoplasm

To determine whether ROS-regulated accumulation of snoRNAs in the cytosol is specific for *Rpl13a* snoRNAs or relevant to snoRNAs as a class of noncoding RNAs, we used RNA sequencing to analyze H9c2 rat cardiomyoblasts following treatment with DOX with or without DPI. We prepared small RNA-sequencing libraries from cytosolic RNA of 35-350 nucleotides in order to capture snoRNAs while minimizing overlap with miRNAs. For each condition, we generated 3 independent libraries that were sequenced on an Illumina HiSeq 2500. Aligned reads were annotated using Ensembl

Rat Build 369, which specifies 560 noncoding RNAs (ncRNA), including 215 sno/scaRNAs. Total raw reads per condition were similar, as were the number of reads aligned to the genome and >99% of annotated reads corresponded to small ncRNA genes (**Table 2.5A**). DOX treatment resulted in a significant increase in both the number and proportion of annotated reads that mapped to box C/D snoRNAs (**Table 2.5A and Figure 2.5A**). Significantly fewer box C/D snoRNAs were recovered with DPI treatment, similar to our findings for the *Rpl13a* snoRNAs. Cytoplasmic box H/ACA snoRNAs and scaRNAs followed the same pattern as box C/D snoRNAs, but did not reach statistical significance (**Figure 2.5A**).

In our RNA-sequencing data, changes in the cytosolic abundance for U32a, U33 and U34 after DOX and/or DPI treatment were similar to those found by RT-qPCR (**Figure 2.5B, lower**). The RNA-seq method was also able to detect a 3-fold increase in cytosolic U35a after DOX treatment, which was not detected by RT-qPCR. This may be due to the superior sensitivity of the RNA-seq method, as U35a is 100-fold less abundant than U34, the most abundant *Rpl13a* snoRNA (**Figure 2.5B, upper**).

Overall, we detected 256 of 560 annotated small ncRNA, including 94 of the 119 annotated box C/D snoRNAs, in the cytoplasm (**Figure 2.5C**). We determined differential representation in the cytoplasm after DOX treatment using normalized read counts and parameters of >2-fold change with false discover rate <0.05. The 105 genes that passed these criteria were all sno/scaRNA with increased cytosolic expression after DOX treatment, 89 of which were box C/D snoRNAs (**Figure 2.5C**). These significantly

increased box C/D snoRNAs account for 95% of the detectable cytoplasmic box C/D snoRNAs, suggesting a strong class effect. Although much fewer, annotated box H/ACA snoRNAs and scaRNA were detected in the cytosol, and more than half also showed significant increases in the cytosol after DOX treatment (**Figure 2.5C**). Together, this RNA-seq data provides evidence that DOX can induce the cytosolic accumulation of a broad range of snoRNAs through a NOX-dependent mechanism.

2.3 CONCLUSIONS

Through RT-qPCR and RNA-seq analyses, we have demonstrated that snoRNAs as a class are not exclusively localized to the nucleus. While the majority of the snoRNAs are localized within the nucleus under basal, homeostatic conditions, snoRNAs are detectable in the cytosol, where their cytosolic abundance is dynamically regulated by oxidative stress. Our results support a model in which DOX treatment induces NOX4D-dependent nuclear superoxide, which leads to snoRNA accumulation in the cytosol (**Figure 2.6**).

2.4 FIGURES

Figure 2.1

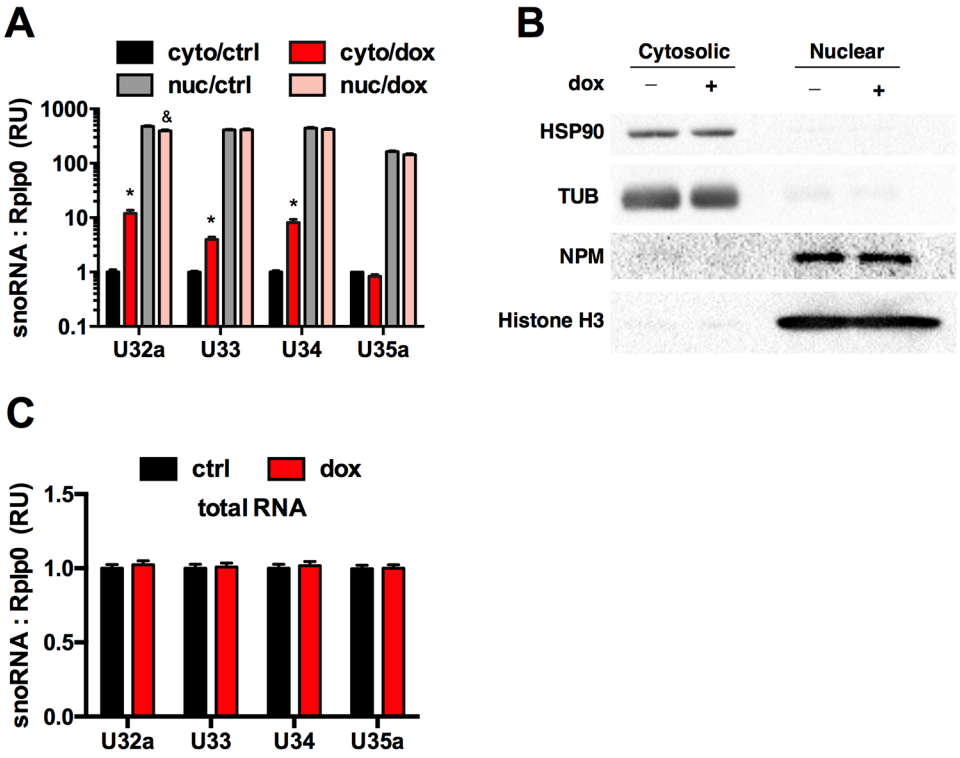

Figure 2.1 Doxorubicin treatment increases cytosolic *Rpl13a* snoRNA levels in cardiomyoblasts. H9c2 cardiomyoblasts were treated with vehicle alone (ctrl) or 20 μM DOX for 1 h. **A-B.** Cytosolic and nuclear extracts were prepared from ctrl and DOX treated cells by sequential detergent extraction. Cytosolic and nuclear RNA were quantified by RT-qPCR with normalization to the control transcript Rplp0. Error bars show 95% confidence interval for n = 3 independent experiments (**A**). Fractions were analyzed by western blot for cytosolic protein markers (HSP90, α-tubulin) and nuclear protein markers (NPM, histone H3) (**B**). **C.** Total RNA was assayed by RT-qPCR with

normalization to the control transcript Rplp0. Error bars show 95% confidence interval for n = 3 independent experiments.

Figure 2.2

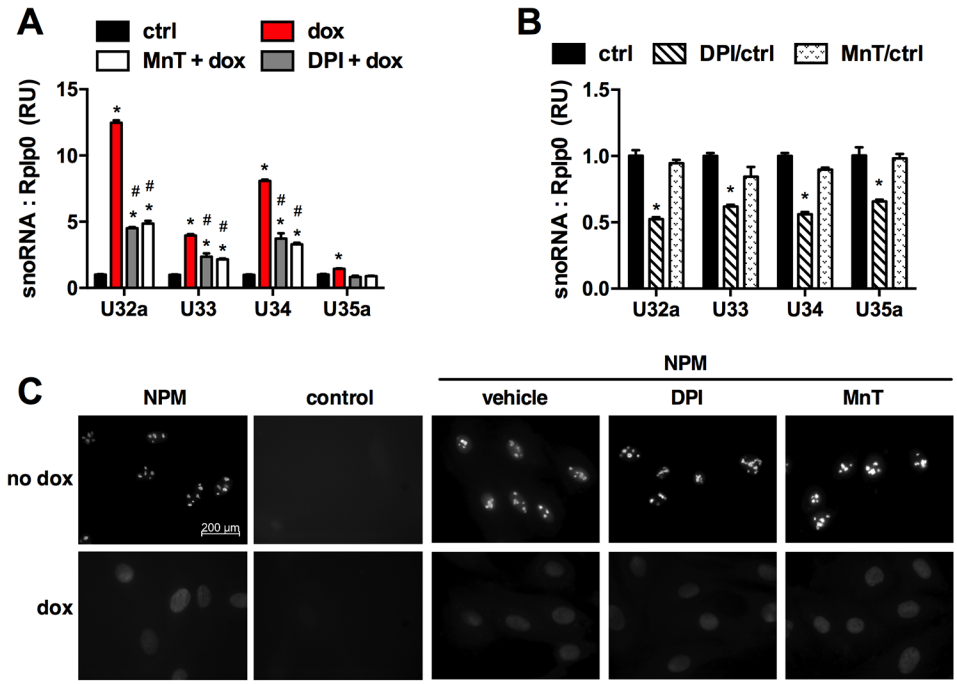

Figure 2.2 Superoxide is necessary for cytosolic *Rpl13a* snoRNA accumulation during doxorubicin treatment. A. Cells were treated for 1 h with vehicle alone (ctrl) or combinations of 20 µM DOX, 500 nM DPI, and 200 µM MnT as shown. Cytosolic RNA was isolated by digitonin extraction and snoRNAs were analyzed by RT-qPCR relative to Rplp0. Error bars show 95% confidence interval for n = 3 independent experiments. **B.** Cells were treated with DPI or MnT alone. Cytosolic RNA was isolated by digitonin extraction and snoRNAs were analyzed by RT-qPCR relative Rplp0. Error bars show 95% confidence interval for n = 3 independent experiments. **C.** Cells were analyzed by immunofluorescence microscopy for detection of NPM under ctrl and 1 h DOX-treated conditions and also in the presence of DPI or MnT. Micrographs show representative fields. Scale bar, 200 µM. *, $p < 0.05$ versus cyto/ctrl; &, $p < 0.05$ versus nuclear/ctrl; #, $p < 0.05$ versus DOX alone.

Figure 2.3

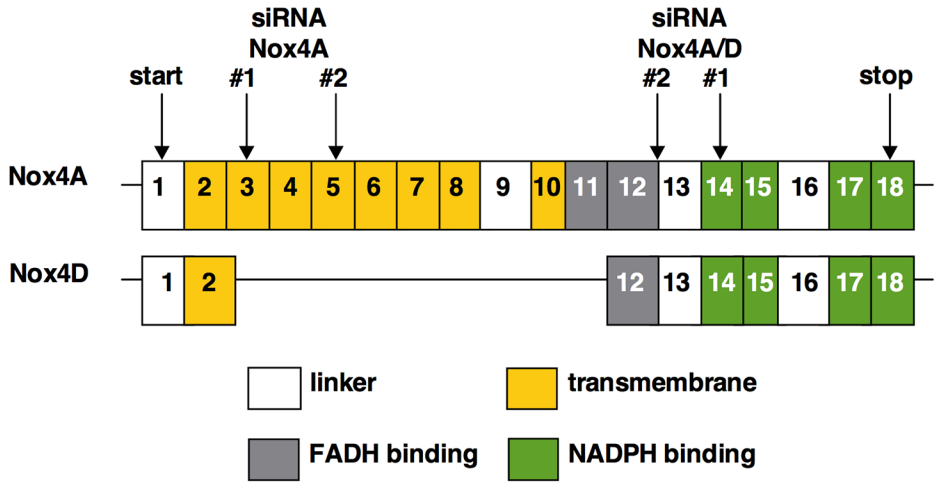

Figure 2.3 Exonic structure of NOX4A and alternatively spliced nuclear form NOX4D. Localization of siRNAs that target NOX4A only (exons 3 and 5) or both NOX4A and NOX4D (exons 12-13 and 14).

Figure 2.4

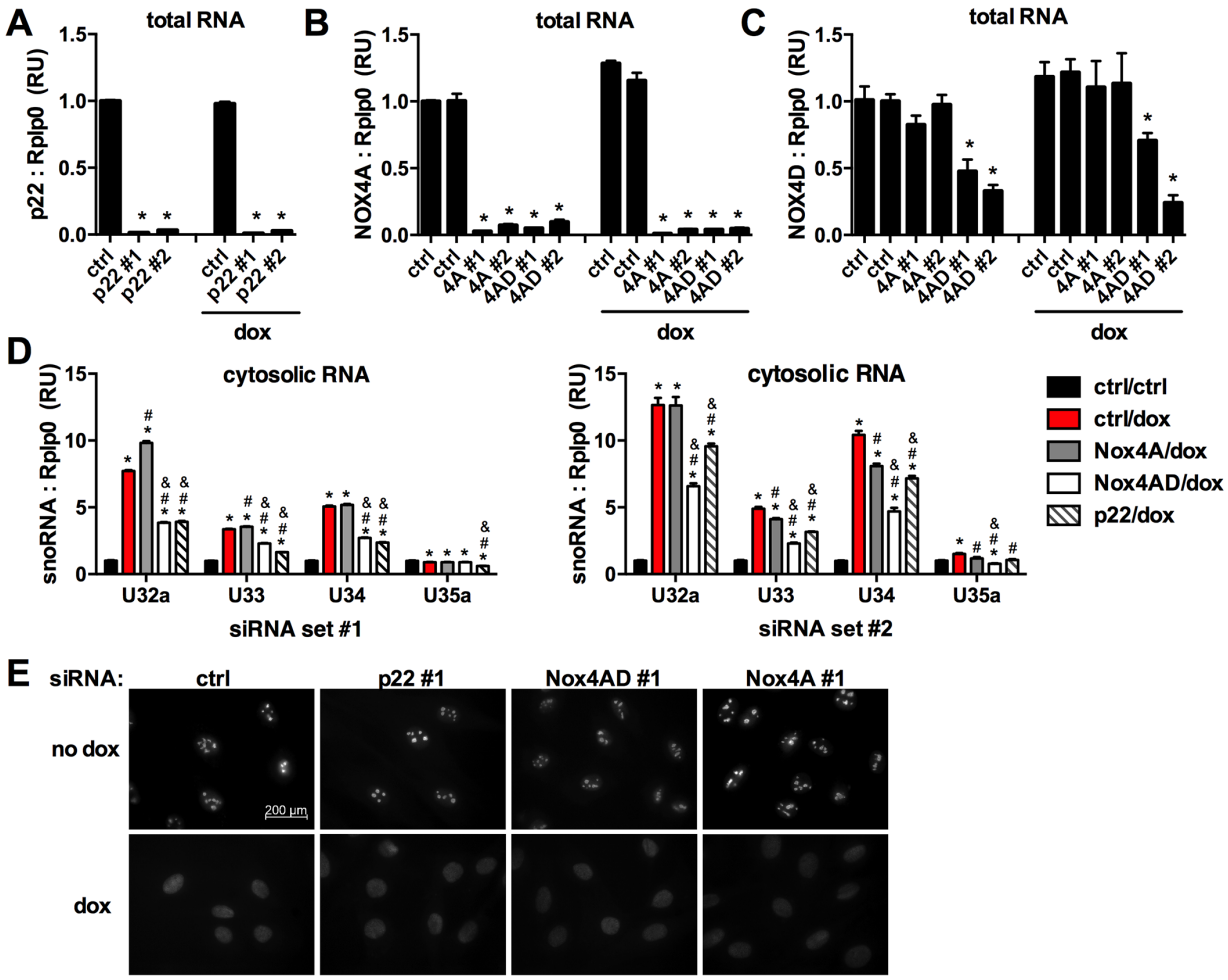

Figure 2.4 NADPH oxidase 4D mediates cytosolic accumulation of *Rpl13a* snoRNAs in response to doxorubicin treatment. A-D. H9c2 cardiomyoblasts were transfected for 24 h with siRNA targeting transcripts as shown: control (ctrl), p22, NOX4A, or NOX4AD. Cells were then treated with 20 µM DOX for 1 h where indicated. RNAs were quantified by RT-qPCR relative to Rplp0. Error bars show 95% confidence interval for n = 3 independent experiments**.** Total RNA was quantified for target knockdown with and without DOX treatment (**A-C**). Cytosolic snoRNAs were quantified after specified siRNA knockdown and DOX treatment (**D**). Cells were treated as above

and analyzed by immunofluorescence microscopy for localization of nucleolar marker NPM. Micrographs show representative fields (**E**). Scale bar, 200 μM. *, $p < 0.05$ versus ctrl; #, $p < 0.05$ versus ctrl/DOX; &, $p < 0.05$ versus NOX4A/DOX.

Figure 2.5

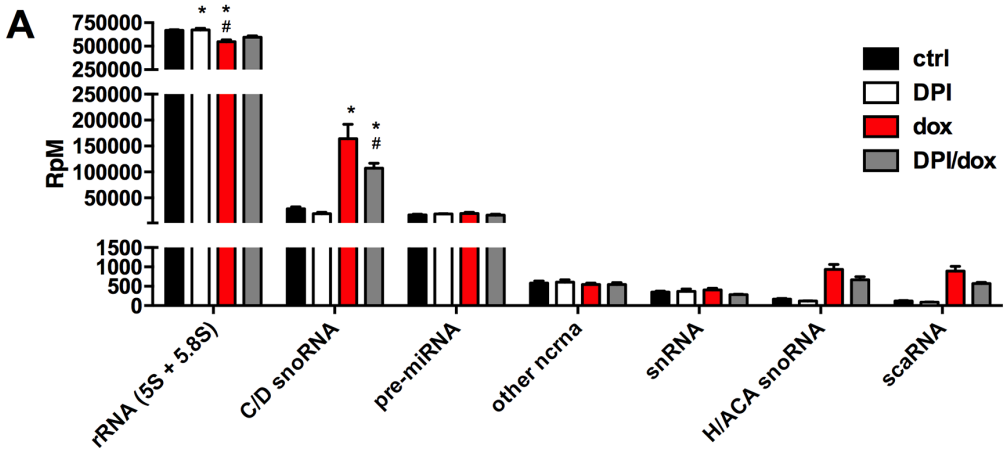

B

RpM	ctrl	DPI	dox	DPI/dox
SNORD32	134.6	90.4	1519.4	880.0
SNORD33	23.7	17.0	110.8	86.4
SNORD34	378.7	259.8	2994.8	1921.1
SNORD35	3.6	1.9	10.1	7.4

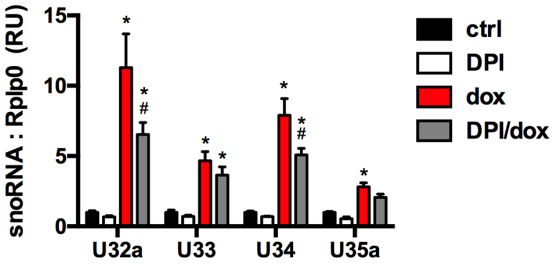

C

	Ensembl ncRNA	detected in cytoplasm	upregulated (dox vs. ctrl)
C/D box	119	94	89
H/ACA box	72	14	9
scaRNA	24	9	7
snRNA	10	8	0
miRNA	324	124	0
rRNA	2	2	0
misc RNA	9	5	0
total	560	256	105

Figure 2.5 SnoRNAs are dynamically regulated in the cytoplasm. H9c2 cardiomyoblasts were treated with 20 μM DOX in the absence or presence of 500nM DPI for 1 h. **A.** Normalized RNA-seq read counts for annotated cytosolic small ncRNA classes. Annotated reads were normalized as reads per million raw reads (RpM) and shown as the mean + standard error (SE) for n = 3 independent experiments . **B.** RNA-seq expression data for the *Rpl13a* snoRNAs in response to treatment with DPI, DOX, or DPI/DOX. Read data are shown as RpM aligned reads to demonstrate the relative abundance of different *Rpl13a* snoRNA species (upper). These values were then further

normalized to the control sample and graphed to show relative expression by treatment (lower). Mean (+SE) for n = 3 independent experiments. **C.** The number of genes annotated for the rat genome (Ensembl ncRNA), number of genes detected experimentally in the cytoplasm by RNA-seq, and number of genes detected in the cytoplasm and up-regulated by DOX versus ctrl are shown by ncRNA subclass. *, $p < 0.05$ for treatment versus ctrl; #, $p < 0.05$ for DPI/DOX versus DOX alone.

Table 2.5A Cytoplasmic RNA-seq reads (total per condition)				
	ctrl	DPI	dox	DPI/dox
Raw	15,777,864	14,321,914	16,038,254	16,539,780
Aligned	15,297,385	13,838,068	15,282,623	15,844,700
Annotated	11,026,233	9,976,388	11,264,042	11,475,445
Annotated ncRNA	10,972,911	9,931,129	11,201,347	11,418,071
sn/sno/scaRNA	453,102	285,808	2,472,756	1,709,804
miRNA	265,594	259,443	305,213	266,277
rRNA (5S + 5.8S)	10,243,718	9,376,317	8,413,350	9,431,538
misc	8,746	8,247	8,236	8,667
snRNA	5,275	4,959	6,105	4,469
scaRNA	1,828	1,221	13,340	8,989
C/D snoRNA	443,462	278,003	2,439,357	1,685,855
H/ACA snoRNA	2,537	1,625	13,954	10,491

Figure 2.6

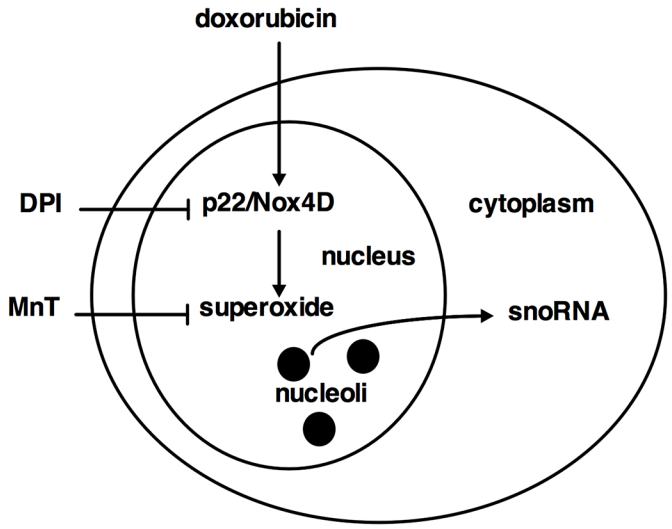

Figure 2.6 Model for cytoplasmic snoRNA regulation. Doxorubicin (DOX) treatment induces high levels of superoxide through the activation of NOX4D enzyme and its regulatory subunit p22. The DOX-induced oxidative stress leads snoRNAs as a class to accumulate in the cytosol. NOX inhibitor DPI and superoxide scavenger MnT inhibit the ability of DOX to increase levels of superoxide and thus blunt the accumulation of snoRNAs in the cytoplasm.

CHAPTER THREE:
NXF3 functions as a nucleocytoplasmic snoRNA transporter

3.1 INTRODUCTION

Following transcription, snoRNAs that are processed from the introns of pre-mRNA or that are generated from independently transcribed units, first move to Cajal bodies where they assemble in to mature snoRNPs, and subsequently to the nucleolus where they encounter nascent rRNA substrates. While *Rpl13a* snoRNAs localize primarily in the nucleus, these and other intronic snoRNAs are readily detected in the cytoplasm under homeostatic conditions [76,89], and they accumulate outside the nucleus during lipotoxic conditions, oxidative stress, and serum starvation [45,47,90]. However, a nucleocytoplasmic trafficking pathway has not yet been identified for the class of snoRNAs.

Nuclear export factor 3 (NXF3) was identified through an shRNA loss-of-function genetic screen in human umbilical endothelial cells (HUVECs) to identify genes required for the cytotoxic response to metabolic stress. Based on its sequence and functional domain similarities, NXF3 is considered to be a member of the nuclear export factor (NXF) family, which includes known mRNA exporter, nuclear export factor 1 (NXF1). However, NXF3 lacks the carboxyl terminal domain, ubiquitin-associated domain (UBA), which is involved in nuclear pore binding, and is required for nuclear export function of other family members [73]. Nonetheless, previous studies have demonstrated that like other family members, NXF3 shuttles between the nucleus and cytoplasm. A leucine

rich nuclear export sequence (NES) was identified within NXF3 that recruits CRM1, thus allowing NXF3 to export cargo through the nucleus [73], but no nuclear import sequence has been defined in the NXF3 sequence. In cells transfected with an HA-tagged form of NXF3 (HA-NXF3), Yang *et al* isolated poly(A) RNA/protein complexes using oligo dT cellulose. They demonstrated that there was a specific interaction between poly(A) RNA and HA-NXF3. This data implicated NXF3 in the nuclear export of mRNA. However, using oligo dT cellulose excludes noncoding RNAs, like snoRNAs, which are not polyadenylated. [73]. The endogenous cargo for NXF3 remains to be defined, including determination of whether it can transport other RNA species like noncoding RNAs. Given that genetic screens implicated both *Rpl13a* snoRNAs NXF3 in lipotoxic response pathways, we hypothesized that NXF3 may also serve as a transporter for snoRNAs.

3.2 RESULTS

3.2.1 NXF3 knockdown protects against lipotoxic cell death in endothelial cells

To identify genes critical for the cell death response to lipotoxicity, we performed a genome-wide loss-of-function shRNA screen in immortalized human umbilical vein endothelial cells (HUVECs), which are sensitive to lipotoxicity. Cells were transduced with pools of lentivirus containing shRNAs targeting expressed human genes and a puromycin selectable marker. HUVECs that survived puromycin selection were then treated for 48 hours in media supplemented with pathophysiological levels of palmitic acid to model lipotoxic conditions. Cells containing an shRNA targeting NXF3 had significantly improved survival compared to cells transduced with a non-targeting, control shRNA (**Fig. 3.1A**). The shRNA targeting NXF3 led to a 72% decrease in NXF3

mRNA levels (**Fig. 3.1B**) and a 28% decrease in NXF3 protein expression (**Fig. 3.1C**), consistent with knockdown of its gene target in these lipotoxicity-sensitive human cells. Together these observations implicate a critical role for NXF3 in the lipotoxic response pathway.

3.2.2 NXF3 knockdown endothelial cells have aberrant *Rpl13a* snoRNA localization

NXF3 is a member of the NXF family that includes the general mRNA export receptor, NXF1. While NXF3 can associate with mRNAs [91], other potential cargo such as noncoding RNAs have not been investigated. Given the important role of *Rpl13a* snoRNAs U32a, U22, U34, and U35a in lipotoxic and oxidative stress-induced cell death, and the observation that these snoRNAs accumulate in the cytoplasm under metabolic stress conditions [45,47], we hypothesized that NXF3 knockdown might affect localization of snoRNAs. We assessed *Rpl13a* snoRNA localization in cytosolic fractions of control- and NXF3-shRNA transduced cells by isolating cytosolic and non-cytosolic fractions using digitonin extraction. Under normal homeostatic growth conditions, levels of cytosolic *Rpl13a* snoRNAs in NXF3 shRNA transduced cells were significantly increased compared with control shRNA transduced cells, while total levels of the snoRNAs did not significantly change (**Figure 3.2A**). Control western blots demonstrated that both nuclear (nucleophosmin) and cytosolic (HSP90, α-tubulin) markers segregated as expected in both control and NXF3 shRNA transduced cells (**Figure 3.2B**). Following treatment with hydrogen peroxide to induce oxidative stress, U32a, U33 and U34 snoRNAs accumulate in the cytoplasm of control shRNA

transduced HUVEC cells (**Figure 3.2C**), consistent with prior observations in other cell types that oxidative stress stimulates cytosolic accumulation of *Rpl13a* snoRNAs [44,47]. In contrast, hydrogen peroxide did not cause further increase in the cytoplasmic levels of snoRNAs in NXF3 shRNA transduced cells. Hydrogen peroxide had no detectable effect on localization of U35a in shRNA transduced HUVEC cells, as has been observed for this less abundant *Rpl13a* snoRNA [47]. Elevated cytoplasmic levels of the snoRNAs under homeostatic conditions in NXF3 shRNA-transduced cells is unlikely to be the result of increased basal oxidative stress or nucleolar stress, since intracellular ROS levels as assessed by dihydroethidium staining (**Figure 3.2D**) and nucleolar integrity as assessed by nucleophosmin staining (**Figure 3.2E**) were unchanged compared to control cells. Our findings that loss-of-function of NXF3 perturbs *Rpl13a* snoRNA subcellular localization indicates that NXF3 functions under homeostatic conditions to maintain the distribution of these non-coding RNAs between the nucleus and cytoplasm. Although NXF3 has been proposed as an mRNA export factor, accumulation of *Rpl13a* snoRNAs in the cytosol in the setting of NXF3 knockdown implicates an additional role for this protein in nuclear import of these small non-coding RNAs.

3.2.3 Knockdown of NXF3 increases cytosolic *Rpl13a* snoRNAs in cardiomyoblasts

We used transient knockdown to confirm our observations regarding NXF3 loss-of-function in an independent cell type and compared the effects of knockdown of NXF3 and related family member, NXF1 (**Figure 3.3A**). Compared to control non-targeting

siRNA, two independent siRNAs directed against NXF3 led to a 93% and 84% decrease, respectively, in NXF3 mRNA levels in H9c2 rat cardiomyoblasts, but did not significantly change levels of NXF1 (**Figure 3.3B, left graph**). Because we found that commercially available antibodies directed against rodent NXF3 are not specific for this family member (not shown), and our attempts to generate a specific antibody that recognizes the rat or murine protein were unsuccessful, extent of knockdown of the endogenous NXF3 protein could not be confirmed. Nonetheless, knockdown of NXF3 mRNA by each siRNA led to a 50 to 200% increase in cytosolic levels of the *Rpl13a* snoRNAs (**Figure 3.3B, right graph**) without perturbing efficiency of fractionation (**Figure 3.3C**). In contrast, siRNA knockdown of NXF1 had no effect on cytosolic levels of *Rpl13a* snoRNAs (**Figure 3.3 D and E**). Thus, accumulation of *Rpl13a* snoRNAs in the cytosol can result from either acute or chronic knockdown of NXF3. This effect is specific for NXF3 and appears consistent across different cell types.

3.2.4 Overexpression of NXF3 decreases cytosolic *Rpl13a* snoRNAs in cardiomyoblasts

Our data are consistent with a model in which NXF3 function is required to maintain low cytoplasmic levels of the *Rpl13a* snoRNAs. To test whether NXF3 promotes movement of snoRNAs between the cytosol and nucleus, we overexpressed murine NXF3 by transiently transfecting NIH 3T3 murine fibroblasts with a GFP-tagged NXF3 construct (NXF3-GFP). As negative controls, we transfected plasmids expressing GFP alone or GFP-tagged NXF1 construct (NXF1-GFP) (**Figure 3.4A**). We consistently observed more efficient transfection with GFP compared to NXF3-GFP and NXF1-GFP,

suggesting that endogenous mechanisms serve to restrict the overall expression of NXF3 and NXF1. Nonetheless, compared to expression of GFP alone, expression of NXF3-GFP decreased cytosolic levels of the *Rpl13a* snoRNAs by 16-34% while there was no significant change in cytosolic *Rpl13a* snoRNAs after NXF1-GFP overexpression (**Figure 3.4B and C**). Additionally, we transiently transfected rat cardiomyoblasts with a non-tagged construct of NXF3. Comparable decreases in U32, U33 and U34 were observed between non-tagged and GFP-tagged NXF3 (**Figure 3.4D**). Together with findings from knockdown of NXF3, our data suggest a model in which NXF3 promotes movement of snoRNAs from the cytoplasm to the nucleus and determines the distribution of the snoRNAs between these cellular compartments.

3.2.5 NXF3 and NXF1 associate with snoRNAs

Since NXF3 is a member of a nuclear RNA transporter family and genetic manipulation of NXF3 impacted *Rpl13a* snoRNA localization, we hypothesized that NXF3 may serve as a snoRNA transporter. A corollary of this hypothesis is that NXF3 should physically interact with the *Rpl13a* snoRNAs. We transiently transfected H9c2 rat cardiomyoblasts NXF3-GFP or GFP alone, and NIH 3T3 murine fibroblasts with NXF3-GFP, NXF1-GFP, or GFP alone and performed immunoprecipitation studies using a GFP antibody, or non-immune IgG as a control. Antibody directed against GFP efficiently and specifically pulled down GFP, NXF3-GFP, or NXF1-GFP, while no GFP, NXF3-GFP or NXF1-GFP was recovered in control IgG immunoprecipitations (**Figure 3.5A and B**). Real-time PCR quantification revealed a 7- to 10-fold increase in *Rpl13a* snoRNA association with immunoprecipitated NXF3-GFP compared to immunoprecipitated GFP in

cardiomyoblasts and 10- to 15-fold increase in fibroblasts (**Figure 3.6A and B**). Interestingly, real-time PCR quantification revealed NXF1-GFP also associated with *the Rpl13a* snoRNAs at similar levels as NXF3-GFP in NIH 3T3 murine fibroblasts. Although only knockdown and overexpression of NXF3 alered snoRNA localization (**Figures 3.3 and 3.4**), our data indicate that both NXF family members are capable of associating with the *Rpl13a* snoRNAs.

We used RNA-sequencing to determine whether NXF3 associates only with *Rpl13a* snoRNAs or with snoRNAs more broadly. We collected RNA from cell lysates before immunoprecipitation (input) and RNA from immunoprecipitates (pulldown) of NIH 3T3 murine fibroblasts transfected with NXF3-GFP. Because most snoRNAs lack polyA tails and do not efficiently prime with random hexamers, they are not well represented in standard libraries prepared using approaches suitable for mRNAs and larger non-coding RNAs [92]. To achieve broad coverage of snoRNAs from both input and pulldown samples, we size-selected RNAs from 30 to 375 nucleotides, a range that would exclude most miRNAs and include most snoRNAs. Libraries were prepared using an Illumina small RNA library preparation kit, sequenced, and aligned to mm9 Refseq Transcripts. We focused our analyses on the non-rRNA sequences, which accounted on average for 55% reads in both input and pulldown samples (**Table 3.6A**). Greater than 98% of non-rRNA reads in the input and pulldown samples aligned to snoRNAs, as expected (**Table 3.6B**). In addition to the *Rpl13a* snoRNAs, NXF3 pulldown recovered many other snoRNAs (**Table 3.6C**), most of which belonged to the box C/D class of snoRNAs, known to be most abundant [93-95]. Approximately 6% of reads in both input

and pulldown aligned to box H/ACA snoRNAs. Due to the methods required to capture snoRNA sequences in library preparation, it was not possible to determine whether NXF3 specifically enriches for snoRNAs over other classes of RNAs. Nonetheless, lack of significant enrichment of specific snoRNA species in pulldown relative to input snoRNAs, indicates that NXF3 broadly associates with this class of small RNAs and does not have specificity for the *Rpl13a* snoRNAs or other particular species (**Table 3.6C**). To validate association with additional box C/D and box H/ACA snoRNAs, we transfected NIH 3T3 fibroblasts with NXF3-GFP or NXF1-GFP or GFP as control, immunoprecipitated with antibody to GFP, and performed RT-qPCR on recovered RNA for abundant snoRNAs for which stem-loop primers were successfully designed. Each of the snoRNAs tested showed similar enrichment in NXF3-GFP and NXF1-GFP pulldown over GFP pulldown, with the exception of SNORA52 (**Figure 3.6C**). Together, our data indicate that NXF3 and NXF1 are capable of associating with a broad range of snoRNAs. Nonetheless, gain- and loss-of-function analyses indicate that only NXF3 functions as a snoRNA nucleocytoplasmic transporter.

3.3 CONCLUSIONS

The endogenous substrates for NXF3, a member of a family of RNA transport proteins, are not well characterized. We show that NXF3 and NXF1 associate with the *Rpl13a* snoRNAs, along with many box C/D and box H/ACA snoRNAs. We demonstrate that gain- and loss-of-function of NXF3, but not NXF1, alters the subcellular distribution of snoRNAs encoded within the *Rpl13a* locus. Together, our data are most consistent with a model in which snoRNAs cycle between the nucleus and cytoplasm and NXF3

efficiently imports snoRNAs from the cytoplasm to the nucleus, a function that helps to maintain low levels of snoRNAs in the cytoplasm under normal homeostatic conditions.

3.4 FIGURES AND TABLES

Figure 3.1

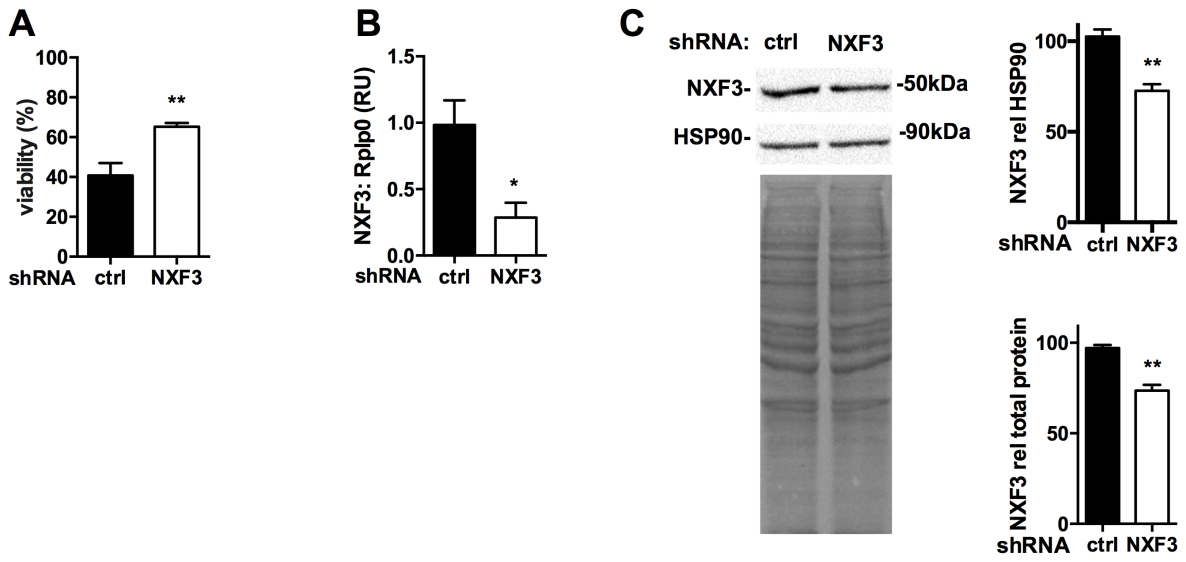

FIGURE 3.1. **Knockdown of NXF3 protects against lipotoxic cell death in endothelial cells.** Human umbilical vein endothelial cells (HUVECs) were transduced with non-targeting (ctrl) or NXF3-targeting shRNA. **A.** Viability following 48 h incubation in media containing 500 μM palmitate. Mean (+ SE) for n = 4. **B.** RT-qPCR quantification of NXF3 mRNA relative to Rplp0 (relative units, RU). Mean (+ SE) for n = 3. **C.** Representative western blot analysis (above) of NXF3 and HSP90 expression or total protein by Ponceau staining with quantification of mean (+SE) NXF3 expression relative to HSP90 or total protein from n = 3 experiments**.** *, $p < 0.05$; **, $p < 0.01$ for NXF3 knockdown vs. ctrl

Figure 3.2

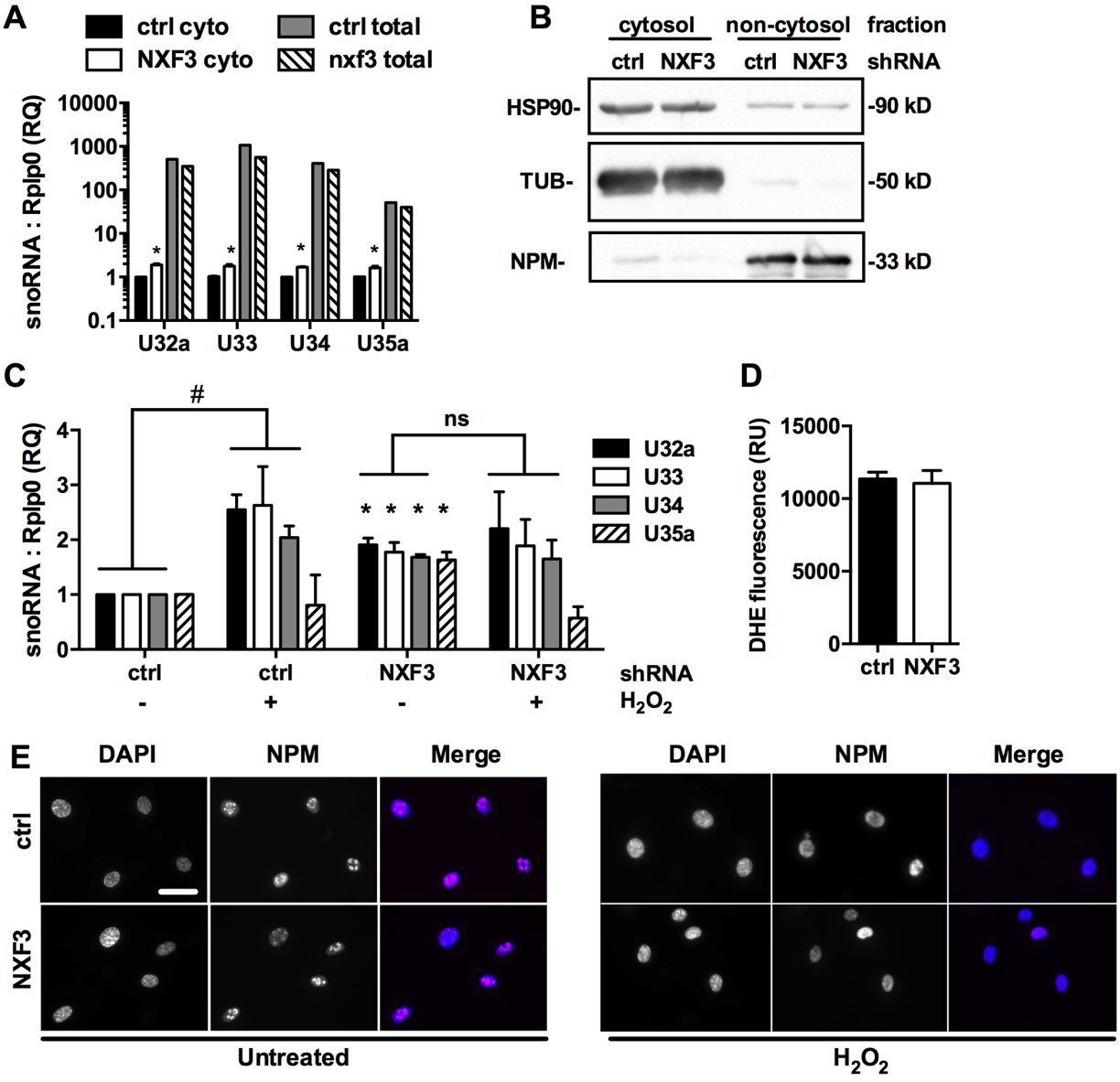

FIGURE 3.2. **NXF3 knockdown alters *Rpl13a* snoRNA localization under basal growth conditions in endothelial cells.** HUVECs were transduced with ctrl or NXF3-targeting shRNA. **A.** RT-qPCR quantification of *Rpl13a* snoRNAs (relative to Rplp0) in cytosolic or total extracts. Mean (+SE) for n = 4 independent experiments. **B.** Representative western analysis of cytosolic and non-cytosolic fractions for cytosolic

(HSP90; α-tubulin, TUB) and nuclear (nucleophosmin, NPM) markers. **C.** Cells were untreated or treated with 1mM H_2O_2 for 4h. RT-qPCR quantification of *Rpl13a* snoRNAs in cytoplasmic extracts relative to Rplp0 and normalized to levels in untreated ctrl shRNA-transduced cells. Mean (+SE) for n = 3. **D.** Quantification of superoxide in untreated ctrl and NXF3-knockdown cells by dihydroethidium (DHE) staining. Mean relative fluorescence (RU) + SE for n = 3. **E.** Representative immunofluorescence staining for NPM and DAPI staining without or following treatment with H_2O_2. Scale bar, 50 μM. *, $p < 0.05$ for NXF3 vs. ctrl shRNA transduced cells; #, $p < 0.05$ for H_2O_2 treated vs. untreated; ns, non-significant

Figure 3.3

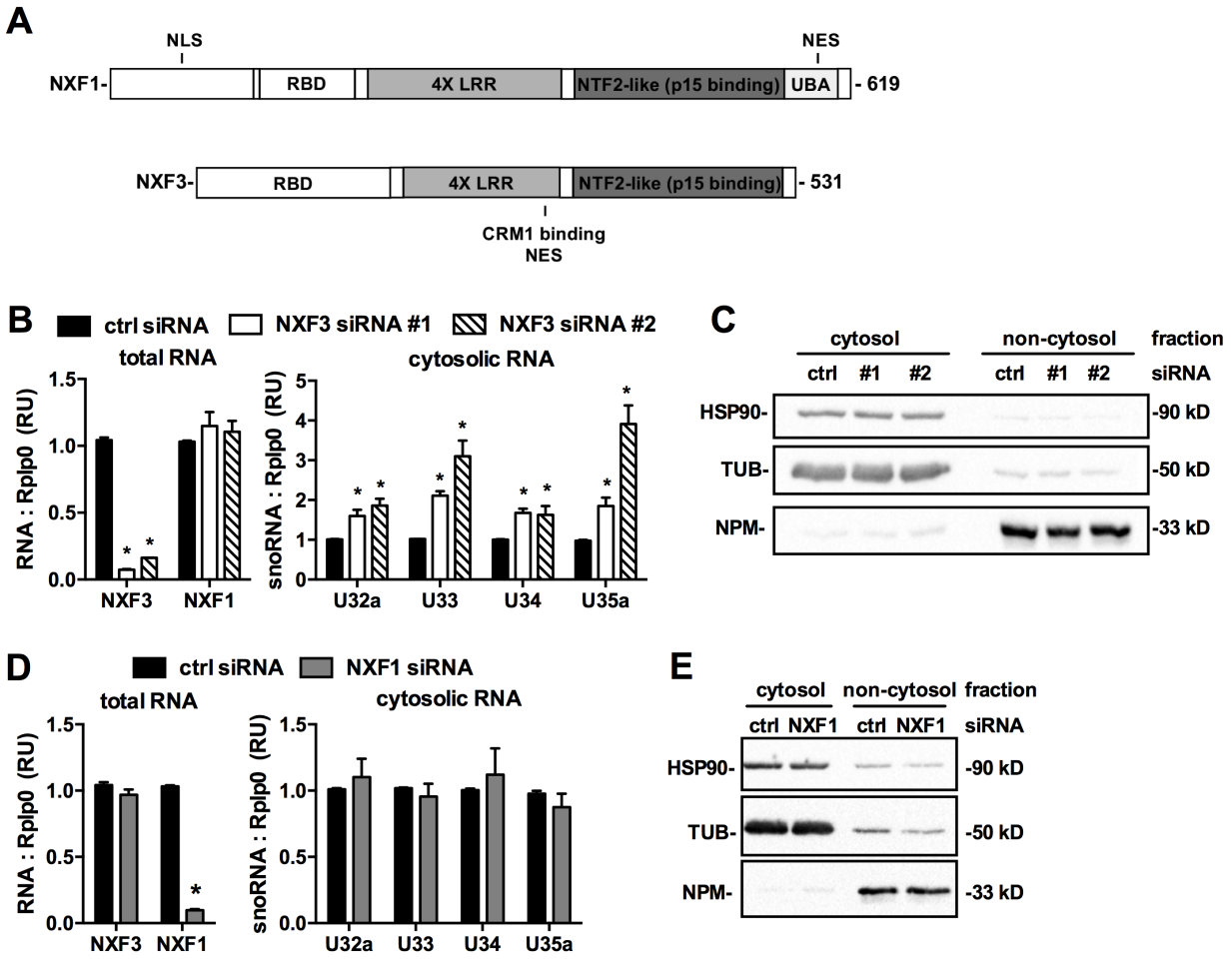

FIGURE 3.3 **Knockdown of NXF3 alters *Rpl13a* snoRNA localization in cardiomyoblasts. A.** Domain structures of NXF1 and NXF3 showing RNA binding domain (RBD), four leucine-rich repeats (4x LRR), sequence with similarity to nuclear transport factor 2 (NTF2-like, involved in p15binding), ubiquitin-associated-like domain (UBA), nuclear localizing sequence (NLS), nuclear export sequence (NES), and CRM1 binding region. **B-D.** H9c2 cardiomyoblasts were transfected with scrambled siRNA (ctrl) or two independent siRNAs targeting NXF3 (**B, C**) or NXF1 (**D, E**). RT-qPCR quantification of NXF3 and NXF1 in total RNA (**B, D,** left graphs) and *Rpl13a* snoRNAs in cytosolic RNA (**B, D,** right graphs) are reported as means (+SE) for n = 3

independent experiments. Representative western analysis (**C, E**) of cytosolic and non-cytosolic fractions for cytosolic (HSP90, TUB) and nuclear (NPM) markers as controls for panels **B** and **D**, respectively. *, $p < 0.05$

Figure 3.4

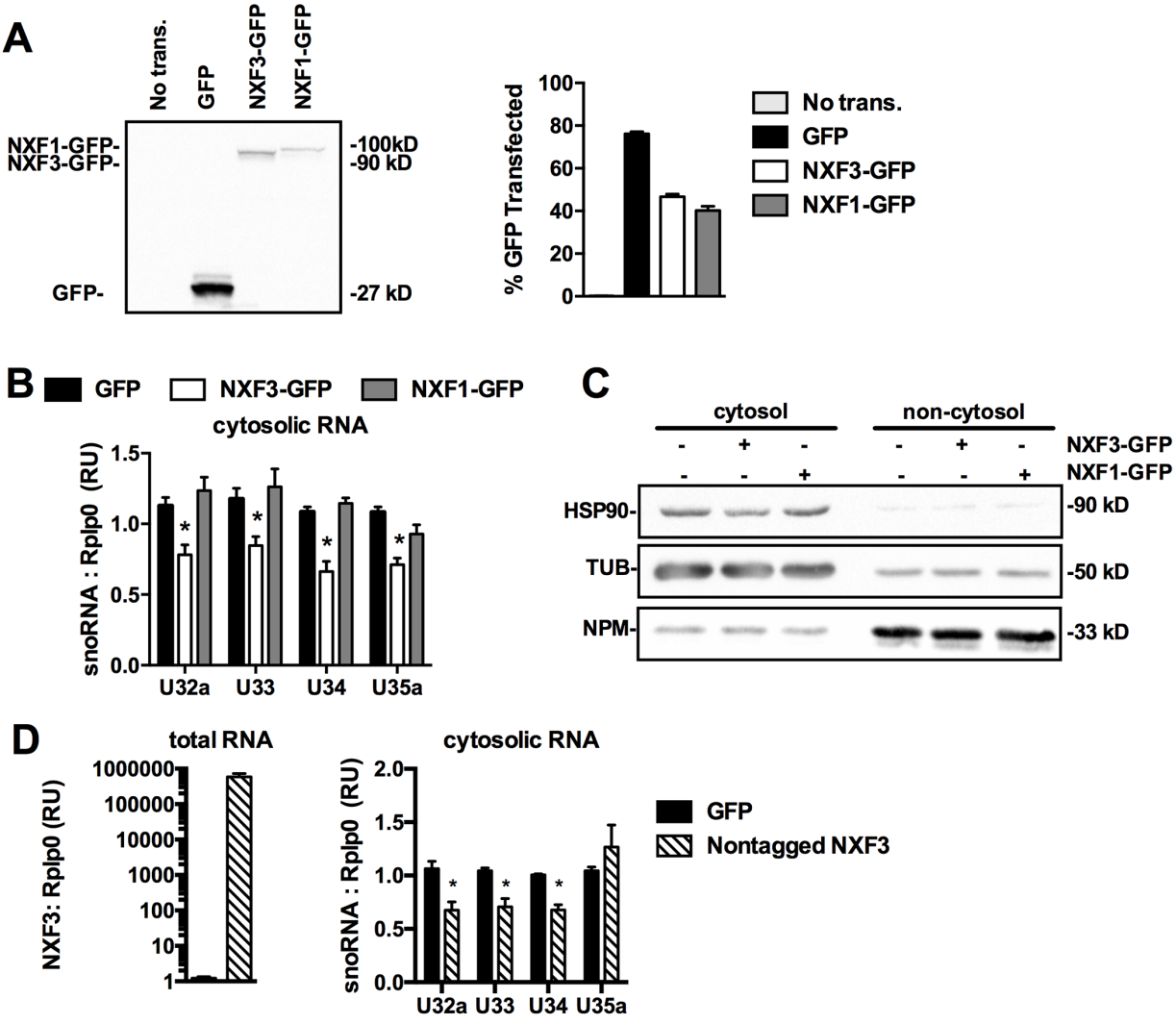

FIGURE 3.4. **Overexpression of NXF3 alters *Rpl13a* snoRNA localization in fibroblasts.** NIH 3T3 fibroblasts were transfected with control plasmid (GFP) or plasmid encoding NXF3-GFP or NXF1-GFP. **A.** Representative western analysis and flow cytometric analysis following transfection. Mean (+SE) for n = 3. **B**. RT-qPCR of cytosolic *Rpl13a* snoRNAs. Mean (+SE) for n = 3. **C**. Representative western analysis of cytosolic and non-cytosolic fractions for cytosolic (HSP90, TUB) and nuclear (NPM) markers. **D.** RT-qPCR quantification of murine NXF3 in total RNA following transfection

of rat cardiomyoblasts (left graph) and corresponding quantification of *Rpl13a* snoRNAs in cytosolic RNA (right graph) are reported as means (+SE) for n = 3. *, $p < 0.05$.

Figure 3.5

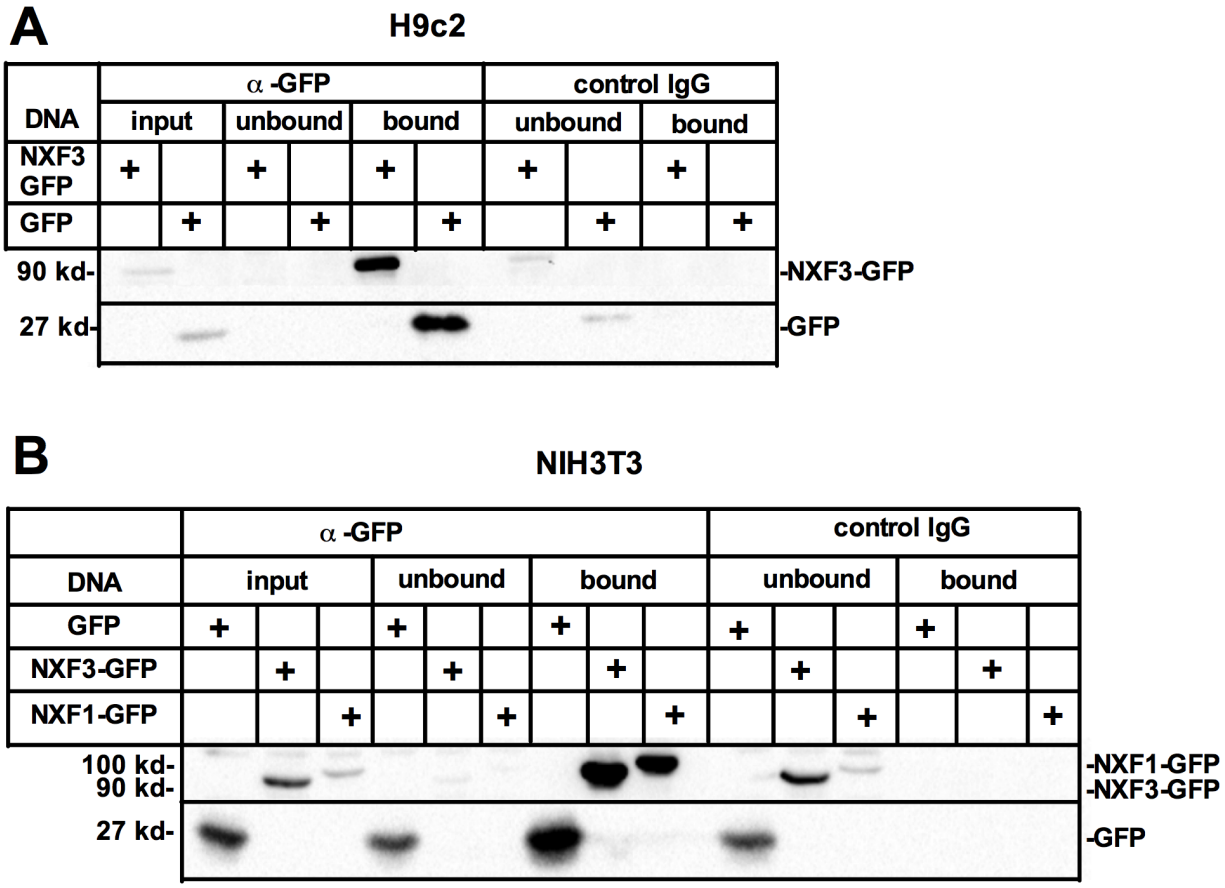

FIGURE 3.5. **NXF3- and NXF1-GFP can be immunoprecipitated using α-GFP.** Immunoprecipitation with α-GFP or rabbit IgG as control was analyzed by western blot analysis using α-GFP. **A.** H9c2 cardiomyoblasts were transfected with control plasmid (GFP) or plasmid encoding NXF3-GFP. **B.** NIH3T3 fibroblasts were transfected with control plasmid (GFP) or plasmid encoding NXF3-GFP. **C.** NIH 3T3 fibroblasts were transfected with control plasmid (GFP) or plasmid encoding NXF1-GFP.

Figure 3.6

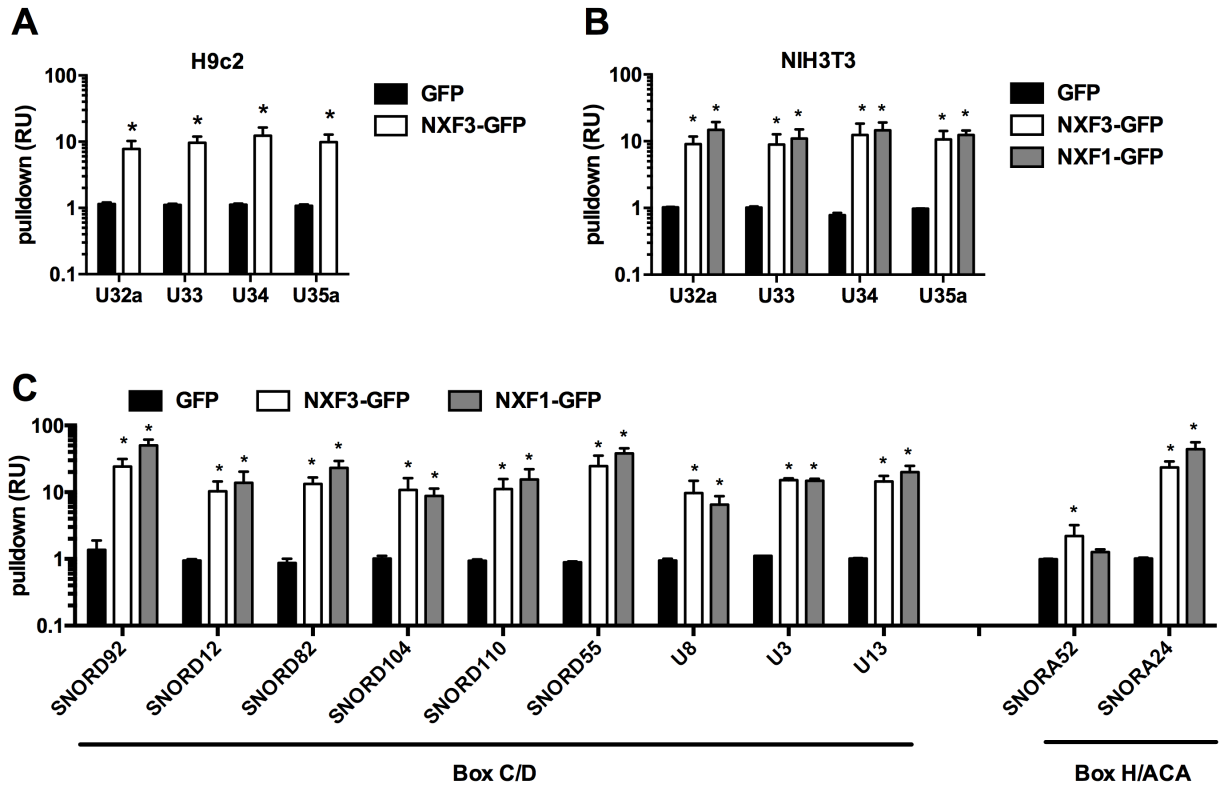

Figure 3.6. **NXF3 and NXF1 associate with snoRNAs**. **A.** Co-immunoprecipitating RNA was isolated and quantified by RT-qPCR for *Rpl13a* snoRNAs in H9c2 cardiomyoblasts transfected with control plasmid (GFP) or plasmid encoding NXF3-GFP. **B,C**. NIH3T3 fibroblasts were transfected with control plasmid (GFP) or plasmid encoding NXF3-GFP or NXF1-GFP. Co-immunoprecipitating RNA was isolated and quantified by RT-qPCR for *Rpl13a* snoRNAs (**B**) and selected box C/D and box H/ACA snoRNAs (**C**). Graphs report enrichment in NXF3-GFP-transfected or NXF1-GFP--transfected cells over GFP-transfected cells. Means (+SE) for n = 3 independent experiments. *, $p < 0.05$

Table 3.6A Quality of RNA Sequencing Data						
	Total reads	**Avg quality**	**% G/C**	**Total aligned**	**% Aligned**	**% rRNA**
Input 1	12622611	36.56	42.81	6914155	54.78	49.32
Input 2	8494636	36.53	43.23	3561964	41.93	36.13
Input 3	15845764	36.57	42.99	7717165	48.70	42.95
Pulldown 1	3321562	36.63	43.40	1498556	45.12	38.85
Pulldown 2	19470767	36.55	42.52	12639529	64.92	59.51
Pulldown 3	13412207	36.55	42.45	6330452	47.20	43.59

Table 3.6B Distribution of Non-Ribosomal RNA Reads			
RNA	**Input (%)**	**Pulldown (%)**	**Significance**
C/D snoRNA	92.45 ± 0.93	91.92 ± 1.69	NS
H/ACA snoRNA	6.26 ± 0.79	6.98 ± 1.50	NS
lncRNA	0.24 ± 0.04	0.33 ± 0.08	NS
miRNA	0.27 ± 0.02	0.19 ± 0.07	NS
mRNA	0.76 ± 0.09	0.59 ± 0.13	NS
Other	0.02 ± 0.00	0.00 ± 0.00	NS

Table 3.6C Most Abundant Immunoprecipitating snoRNAs

Gene ID	LSMean (Pulldown)	LSMean (Input)	Enrichment (pulldown/input)	FDR	P-value	Significance
Snord55	421533.33	422930.00	1.00	1.00	0.84	NS
Snord44	299548.00	218320.33	1.37	0.99	0.87	NS
Z23	229492.67	218334.00	1.05	0.99	0.56	NS
Snord24	208143.67	156536.67	1.33	0.99	0.90	NS
Snord2	144321.67	150285.33	0.96	1.00	0.64	NS
Snora48	120987.00	114743.00	1.05	0.99	0.87	NS
Snord45	97189.00	82084.33	1.18	0.99	0.77	NS
Z19	76795.67	86895.67	0.88	0.99	0.57	NS
Z15	70041.33	78718.67	0.89	0.99	0.64	NS
Snord14e	56763.00	51011.67	1.11	0.99	0.90	NS
Snord4a	50187.00	32887.00	1.53	1.00	0.91	NS
Snord96a	29898.00	36448.00	0.82	1.00	0.53	NS
Snord45c	26526.00	17509.67	1.51	0.99	0.99	NS
Snord74	23828.33	20331.67	1.17	0.99	0.74	NS
Snord32a	23639.33	36071.67	0.66	1.00	0.62	NS
Snord14d	18182.33	14849.67	1.22	0.99	0.79	NS
Snord14c	14650.00	11996.67	1.22	0.99	0.77	NS
Snord73	11345.33	10193.33	1.11	0.99	0.61	NS
Snord34	10821.67	9770.33	1.11	1.00	0.61	NS
Snord95	9882.33	7793.67	1.27	1.00	0.84	NS
Snord1b	8164.00	8715.67	0.94	1.00	0.49	NS
Snord35a	5050.33	7777.33	0.65	1.00	0.43	NS
Snord113	4508.67	5383.67	0.84	0.99	0.81	NS
Snord82	4491.33	3655.33	1.23	1.00	0.97	NS
Snord104	3567.00	2764.67	1.29	1.00	0.98	NS
DQ267100	2406.67	3323.33	0.72	0.99	0.50	NS
Snord100	2392.67	2097.33	1.14	1.00	0.76	NS
Snord1c	2302.00	2378.67	0.97	1.00	0.42	NS
Snord12	2044.33	862.67	2.37	1.00	0.34	NS
Snord33	1497.33	881.00	1.7	1.00	0.87	NS
Snord15b	1280.00	1128.67	1.13	1.00	0.99	NS
Snord123	1268.67	1322.00	0.96	1.00	0.45	NS
Rnu73b	980.33	984.00	1.00	1.00	0.47	NS
DQ267102	963.33	1123.33	0.86	0.99	0.74	NS
Snord92	746.67	466.00	1.60	1.00	0.88	NS
Snord37	650.00	674.67	0.96	0.99	0.61	NS
AF357426	647.33	366.67	1.77	0.99	0.98	NS
AF357425	505.67	525.67	0.96	0.99	0.81	NS
Snord15a	478.00	545.67	0.88	1.00	0.69	NS
AF357355	317.33	388.00	0.82	0.99	0.87	NS
Snord110	297.33	158.00	1.88	1.00	0.62	NS
Snora24	271.51	742.24	0.37	1.00	0.07	NS
Z21	220.00	144.67	1.52	0.99	0.93	NS
Gm24148	198.00	134.00	1.48	1.00	0.78	NS
Snord22	189.33	340.00	0.56	1.00	0.24	NS
Snora52	180.00	212.67	0.85	1.00	0.42	NS
Snora16a	163.33	144.00	1.13	1.00	0.75	NS

CHAPTER FOUR:
NXF3 as a point of regulation of transport

4.1 INTRODUCTION

Eukaryotic cells are divided into distinct compartments that have specific functions. This compartmentalization is important in determining the environments in which proteins and RNA operate. The localization of proteins and RNA within the cell can impact their functions. Therefore, transport between organelles and the resulting subcellular distribution is tightly regulated [96]. An understanding of the regulation of the nucleocytplasmic transport of NXF3 and the snoRNAs, may provide insights into snoRNA roles outside of the nucleus.

Forskolin (FSK) is a labdane diterpene drug that activates adenylyl cyclase, leading to an increase in levels of intracellular cyclic AMP [97]. Protein kinase A (PKA) activation is dependent on cyclic AMP, thus allowing the catalytic subunits of PKA to phosphorylate many substrate proteins. The resulting phosphorylation of proteins can result in their translocation. For example, phosphorylation can increase the affinity between cargo and its specific import factor, thus increasing nuclear import. Additionally, phosphorylation of a protein can induce a conformational change that exposes an NLS. It is not known whether FSK impacts snoRNA trafficking or the function of NXF3 through phosphorylation. However, it is important to note that forskolin can also activate exchange proteins activated by cAMP and activate calcium channels [98-101].

Our work has shown that distribution of snoRNAs between the nucleus and cytoplasm is perturbed by treatment with doxorubicin (DOX). DOX is an anthracycline chemotherapy drug that induces high levels of reactive oxygen species (ROS) [47,83]. The mechanism whereby ROS in general or DOX in specific alters distribution of snoRNAs is not known.

The experiments described below were undertaken to characterize the effects of FSK and DOX on snoRNA localization and to determine whether effects of these agents may be mediated through the actions of NXF3.

4.2 RESULTS

4.2.1 Forskolin decreases cytosolic *Rpl13a* snoRNAs and increases NXF3-*Rpl13a* snoRNA association

Treatment of H9c2 cardiomyoblasts or NIH 3T3 fibroblasts for 1 h with FSK significantly decreased cytosolic *Rpl13a* snoRNA levels compared to DMSO-treated controls (**Figure 4.1**). To test whether FSK affects NXF3 localization or its association with snoRNAs, we transfected NIH 3T3 fibroblasts with a plasmid for expression of NXF3-GFP. Similar to our findings with untransfected cells, and independent of the effects of NXF3 overexpression itself, cells over-expressing NXF3-GFP had decreased cytosolic snoRNA abundance following 1 h treatment with FSK (**Figure 4.2 A and B**). Moreover, FSK increased association of NXF3-GFP with the *Rpl13a* snoRNAs (**Figure 4.2C**). Concomitantly, immunofluorescence microscopy revealed increased nuclear localization of NXF3-GFP (**Figure 4.2D**). Together these observations are consistent with a model

of NXF3-mediated trafficking of snoRNAs from the nucleus to the cytoplasm that is regulated by FSK.

4.2.2 NXF3 phosphorylation does not change during forskolin treatment

FSK is a natural compound that activates cyclic AMP signaling through both PKA-dependent and PKA-independent mechanisms that could lead to downstream phosphorylation cascades. Moreover, cAMP regulation of nucleocytoplasmic transport can be mediated through post-translational modifications of transporters, such as phosphorylation. Using algorithms for prediction of phosphorylation sites, we identified several potential sites for phosphorylation by PKA and other kinases [http://kinasephos2.mbc.nctu.edu.tw/]. We performed an immunoprecipitation of NXF3-GFP before and after FSK treatment. Monoclonal antibodies specific for threonine-, serine-, or tyrosine-phosphorylation sites was used to determine whether NXF3-GFP phosphorylation levels change after FSK treatment. While each of these antiphospho-antibodies recognizes immunoprecipitated NXF3-GFP, we did not detect any significant changes in phosphorylation levels after FSK treatment (**Figure 4.3**).

4.2.3 Doxorubicin increases cytosolic *Rpl13a* snoRNAs and decreases NXF3-*Rpl13a* snoRNA association

Previously, we showed that treatment of cells with the chemotherapy drug doxorubicin (DOX) induces nucleolar stress and increases cytosolic *Rpl13a* snoRNAs [47]. We hypothesized that DOX treatment might also regulate association between NXF3-GFP and the *Rpl13a* snoRNAs. As observed previously in untransfected cells [45,47], treatment

with DOX for 1 h increased cytosolic snoRNA levels in NXF3-GFP overexpressing cells (**Figure 4.4 A and B)**. Furthermore, DOX decreased association between NXF3-GFP and the *Rpl13a* snoRNAs (**Figure 4.4C**). Although the wide fluorescence emission range of DOX confounds immunofluorescence microscopy approaches, analysis of subcellular fractions of NXF3-GFP expressing cells revealed that the drug decreases nuclear localization of NXF3 (**Figure 4.4D**). Thus, a treatment that promotes cytoplasmic accumulation of snoRNAs also perturbs localization of NXF3 and its association with snoRNA cargo.

4.2.4 Forskolin effect on snoRNA localization is dependent on NXF3

To determine whether the FSK- or DOX-induced changes in localization of *Rpl13a* snoRNAs were dependent on NXF3, H9c2 rat cardiomyoblasts were transiently transfected with siRNA to knockdown NXF3 (**Figure 4.5A and C**) and then treated with FSK or DOX. Although FSK decreased cytosolic *Rpl13a* snoRNAs as expected in control siRNA-transfected cells, this effect was abrogated when NXF3 was knocked down (**Figure 4.5B**). In contrast, DOX-induced increases in cytosolic U32a, U33, and U34 were preserved in the setting of knockdown of NXF3 (**Figure 4.5D**). As reported previously, DOX did not cause cytosolic accumulation of U35a [47]. Taken together, our data are most consistent with a model in which FSK action to diminish cytoplasmic snoRNAs is dependent on NXF3.

4.3 CONCLUSIONS

Our studies provide new evidence that FSK regulates the association of snoRNAs and the transport protein, NXF3, as well as the trafficking of both snoRNAs and NXF3. Furthermore, NXF3 is required for acute regulation of nuclear snoRNA import by FSK. On the other hand, lack of dependence of DOX-stimulated snoRNA export on NXF3 suggests that this transport limb may not depend on NXF3. This data suggest a model in which snoRNAs are continuously cycled between the nucleus and cytosol under basal conditions. NXF3 efficiently returns the snoRNAs back to the nucleus. FSK treatment increases the association between NXF3 and the snoRNAs, and signals the NXF3-snoRNA complex to increase its localization into the nucleus, thus depleting the cytosolic levels of snoRNAs. While DOX treatment raises cytosolic levels of snoRNAs, this function appears to be indpenedent of NXF3 function (**Figure 4.6**).

4.4 FIGURES

Figure 4.1

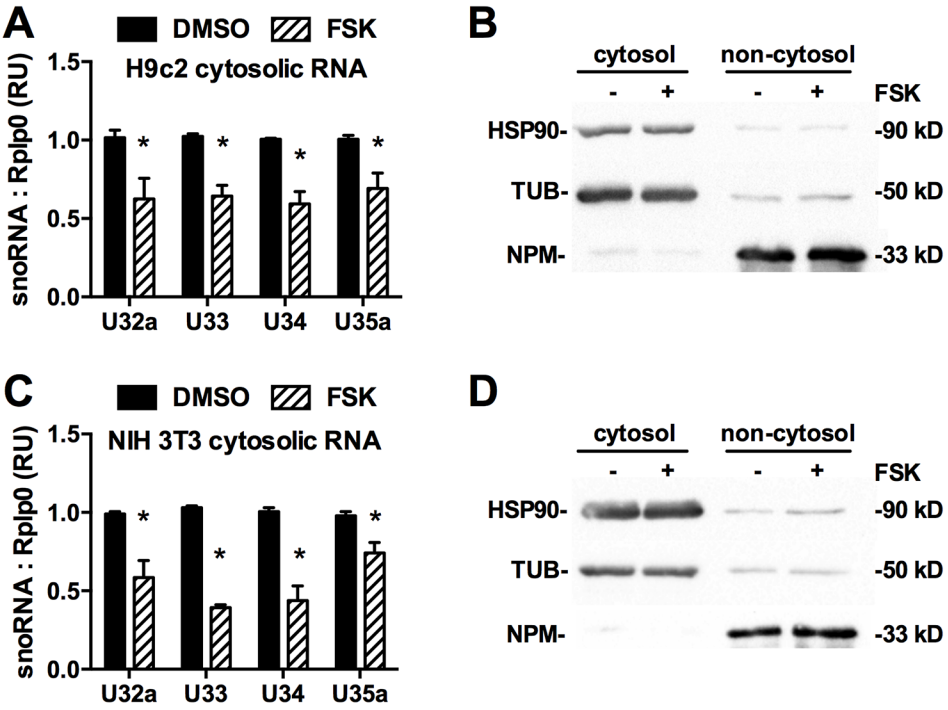

Figure 4.1 **Forskolin decreases cytosolic *Rpl13a* snoRNA levels.** H9c2 cardiomyoblasts (**A, B**) and NIH 3T3 fibroblasts (**C, D**) were treated with 10 μM forskolin (FSK) or vehicle (DMSO) for 1 h. **A, C.** Quantification of cytosolic *Rpl13a* snoRNAs relative to Rplp0 by RT-qPCR. Mean (+SE) for n = 3 independent experiments **B, D.** Representative western analysis of cytosolic and non-cytosolic fractions for cytosolic (HSP90, TUB) and nuclear (NPM) markers. *, $p < 0.05$

Figure 4.2

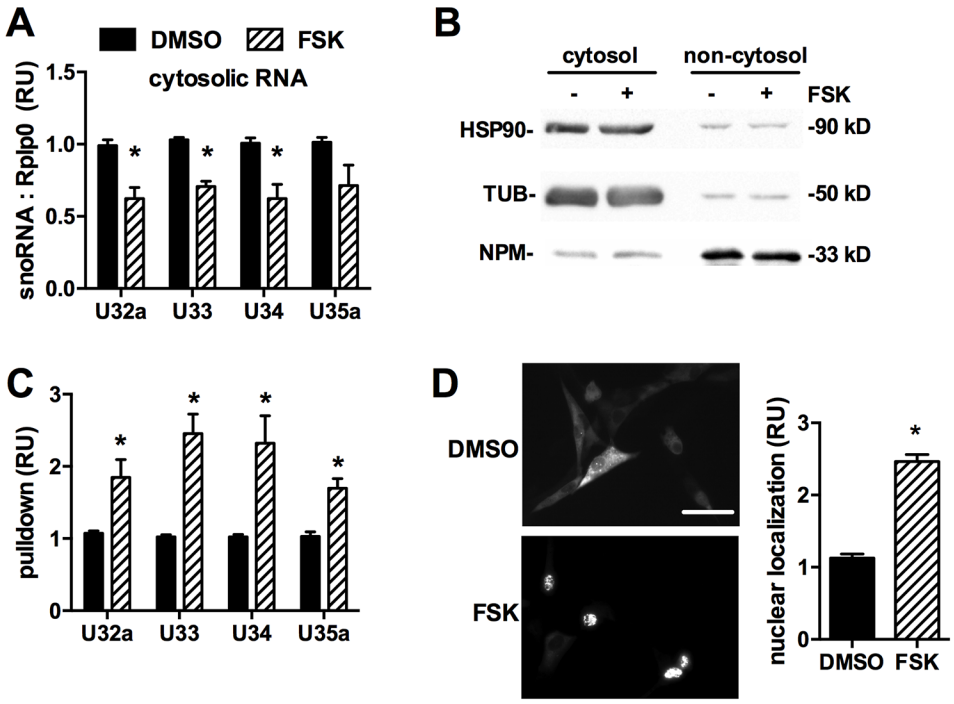

Figure 4.2 **Forskolin increases NXF3-GFP-snoRNA association and nuclear localization of NXF3-GFP**. NIH 3T3 fiboroblasts were transfected with control plasmid (GFP) or plasmid encoding NXF3-GFP and subsequently treated with vehicle (DMSO) or 10 μM FSK for 1 h. **A.** Cytosolic *Rpl13a* snoRNAs were quantified by RT-qPCR relative to Rplp0 in DMSO treated cells. Mean (+SE) for n = 3 independent experiments. **B**. Representative western analysis of cytosolic and non-cytosolic fractions for cytosolic (HSP90, TUB) and nuclear (NPM) markers. **C**. Following immunoprecipitation with α-GFP, *Rpl13a* snoRNAs were quantified by RT-qPCR. Graph reports snoRNA abundance in immunoprecipitates from NXF3-GFP-transfected cells relative to GFP-transfected controls. Mean (+SE) for n = 3 independent experiments. **D**. Representative mmunofluorescence micrographs show NXF3-GFP localization. Graph reports summary

immunofluorescence data from n = 3 independent experiments. Cells were counted from 20 independent fields per treatment. Scale bar, 50 μM. *, $p < 0.05$.

Figure 4.3

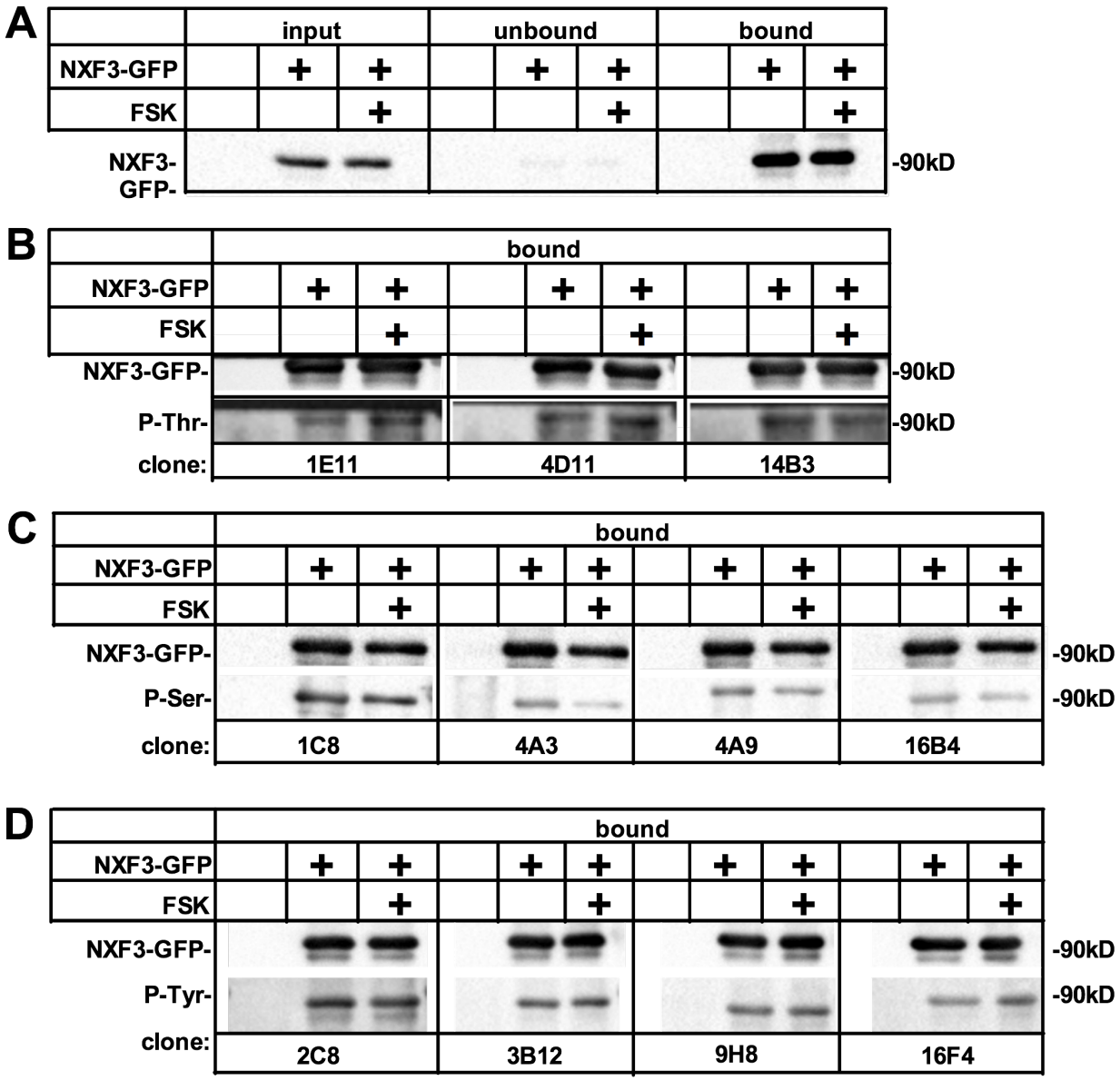

Figures 4.3 **Forskolin does not change NXF3-GFP phosphorylation levels.** NIH 3T3 fibroblasts were transfected with a plasmid encoding NXF3-GFP and compared to untreated, non-transfected cells. Transfected cells were treated with or without 10 μM FSK for 1 h. **A.** Representative western blot of immunoprecipitation with α-GFP was

analyzed using α-GFP to demonstrate efficient pulldown of NXF3-GFP. **B-D**. Representative western blots of immunoprecipitation with α-GFP was analyzed using α-GFP or specified anti-phospho-threonine (**B**), anti-phospho-serine (**C**), and anti-phospho-tyrosine (**D**) antibodies.

Figure 4.4

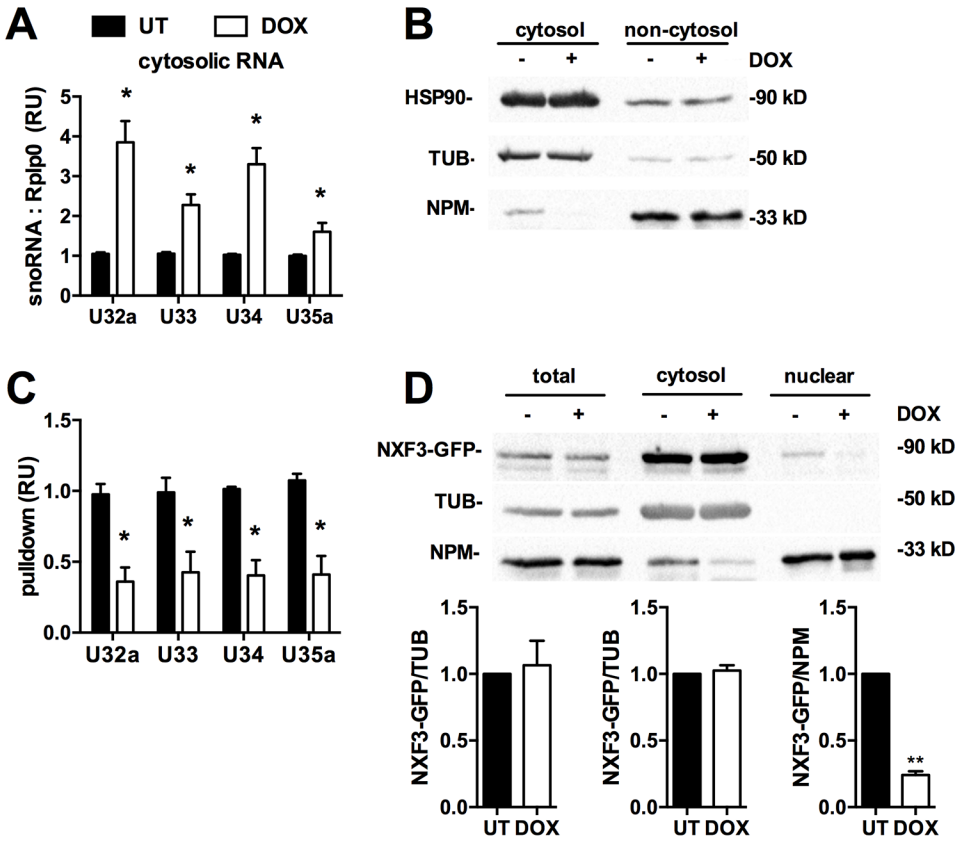

Figure 4.4 **Doxorubicin increases cytosolic snoRNAs and decreases NXF3 association with *Rpl13a* snoRNAs.** H9c2 cardiomyoblasts were transfected with plasmids encoding NXF3-GFP or GFP as control and then were untreated (UT) or treated with 20 μM doxorubicin (DOX) for 1 h. **A, B.** Cytosolic snoRNAs quantified by RT-qPCR relative to Rplp0 in NXF3-GFP-transfected cells. Graph (**A**) shows mean (+SE) for n = 4 independent experiments. Representative western analysis of cytosolic and non-cytosolic fractions for cytosolic (HSP90, TUB) and nuclear (NPM) markers (**B**). **C.** Following immunoprecipitation with α-GFP, *Rpl13a* snoRNAs were quantified by RT-qPCR. Graph reports snoRNA abundance in immunoprecipitates from NXF3-GFP-transfected cells relative to GFP-transfected controls. Mean (+SE) for n = 3. **D.** NXF3-

GFP localization before and after DOX treatment assessed by digitonin extraction. Representative western analysis and graphs showing summary densitometric analysis from n = 3 independent experiments. *, $p < 0.05$; **, $p < 0.0001$

Figure 4.5

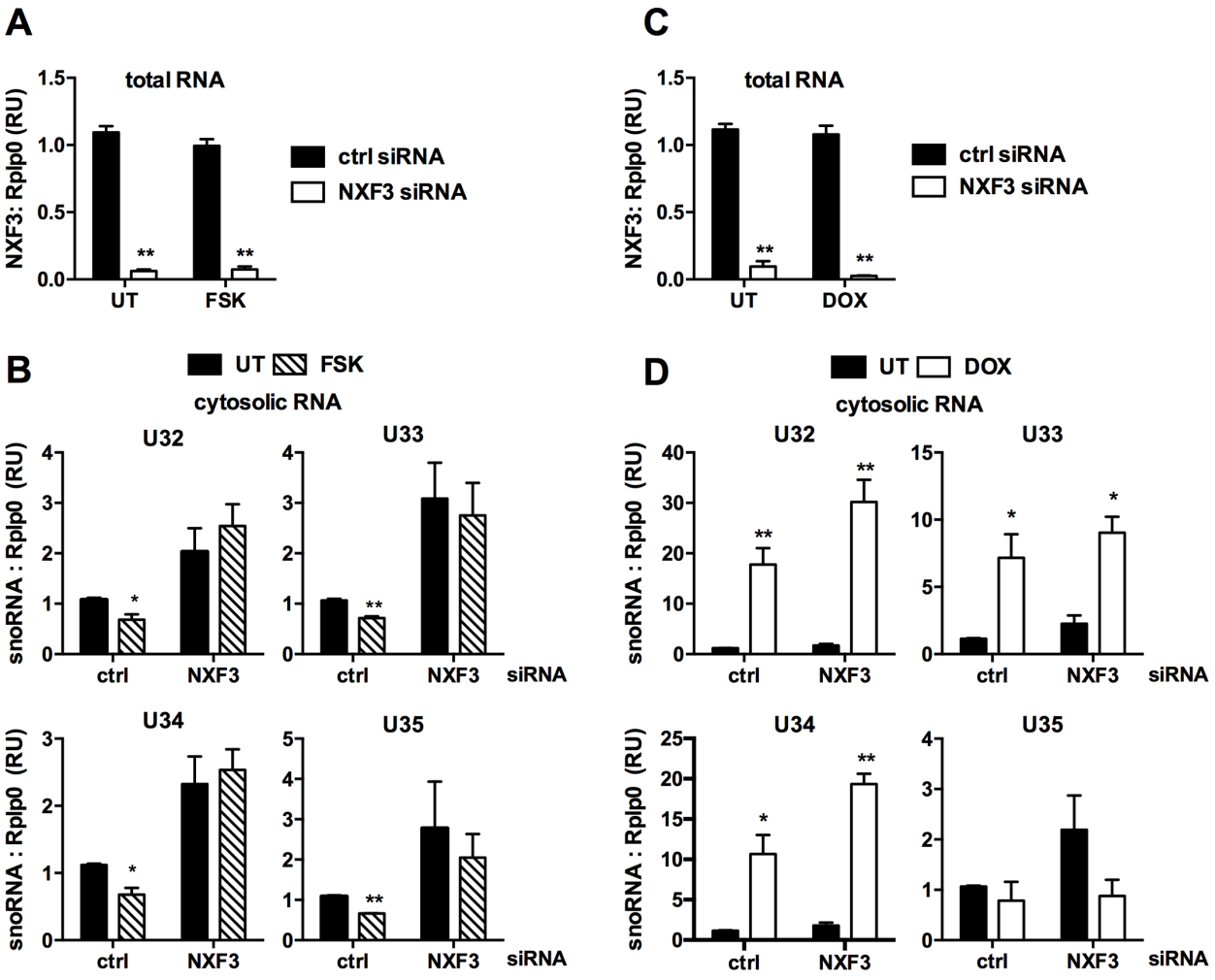

Figure 4.5 **Forskolin effect on snoRNA localization is dependent on NXF3.** H9c2 cardiomyoblasts were transfected with scrambled siRNA (ctrl) or siRNA targeting NXF3 and subsequently treated for 1 h with 10 µM FSK (**A, B**) or 20 µM DOX (**C, D**). **A, C.** RT-qPCR quantification of total NXF3 relative to Rplp0. **B, D.** RT-qPCR quantification of cytosolic *Rpl13a* snoRNAs relative to Rplp0. Graphs show mean (+SE) for n = 3 independent experiments. * $p < 0.05$; ** $p < 0.01$

Figure 4.6

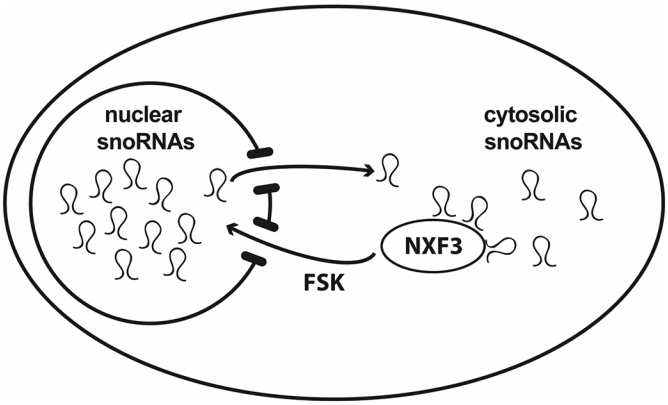

Figure 4.6 **Model for NXF3 function.** SnoRNAs cycle between the nucleus and cytoplasm under homeostatic conditions. NXF3 functions as an importer, efficiently returning snoRNAs to the nucleus and maintaining a high concentration of snoRNAs in the nucleus relative to the cytoplasm. FSK treatment enhances return of NXF3-snoRNA complexes to the nucleus, further depleting cytosolic levels of snoRNAs.

CHAPTER FIVE:
Summary and Discussion

5.1 Summary

There is evidence for a growing number of non-canonical roles for snoRNAs. The *Rpl13a* snoRNAs have been shown to mediate the cellular response to metabolic stress *in vitro* and *in vivo* [45,61]. Moreover, these and other snoRNAs accumulate in the cytosol in response to lipotoxic stress and general oxidative stress [45,47]. The mechanisms through which snoRNAs act in metabolic stress responses and their RNA targets in this response are not known. However, it is possible that movement of snoRNAs out of the nucleus during these stress response pathways enables snoRNAs to target RNAs in other cellular compartments, including mRNAs. Experimentally disrupting the nucleocytoplasmic trafficking of the snoRNAs could be used to probe the functions of snoRNAs in the cytosol. However, mechanisms that govern snoRNA localization and transport between the nucleus and cytoplasm are poorly understood. Herein, we demonstrate that the cytosolic accumulation of snoRNAs is regulated by enzyme NOX4D during doxorubicin treatment. We have also identified NXF3 as a potential snoRNA nucleocytoplasmic transporter.

5.2 Cytosolic snoRNAs

Previous studies using traditional methods like *in situ* hybridization and cell fractionation with detection by northern blotting have shown that snoRNAs localize solely in the nucleus within Cajal bodies and nucleoli, where they perform their canonical function of modifying snRNA and rRNA, respectively. Our experiments in which we coupled high

sensitivity methods of RT-qPCR or RNA-seq to cell fractionation approaches, demonstrate for the first time that a broad range of snoRNAs is easily detectable in the cytoplasm under basal, homeostatic conditions. The accumulation of snoRNAs in the cytoplasm after oxidative stress induced by DOX is rapid and significant. Prior studies demonstrated that independently transcribed, capped snoRNAs U3, U8 and U13 traffic between the nucleus and cytoplasm. We show that in addition to these snoRNAs, intronic, uncapped snoRNAs follow this itinerary and are present in the cytoplasm.

Our data demonstrate that the localization of snoRNAs as a class is regulated at least in part by NOX and superoxide. Furthermore, our knockdown studies implicate nuclear localized NOX4D as a key regulator of the nuclear-cytosolic partitioning of *Rpl13a* snoRNAs. Under homeostatic conditions, most intronic snoRNAs localize in the nucleolus, suggesting that following synthesis these snoRNAs either remain within the nucleus, or if they traffic to the cytoplasm, they are efficiently returned to the nucleus. A model of tight regulation of cytosolic snoRNA levels is further supported by our lab's prior observation that mutant cells with 50% reduction of nuclear *Rpl13a* snoRNAs maintain wild-type cytosolic levels of these snoRNAs [46]. The rapid accumulation of snoRNAs in the cytosol following DOX treatment suggests that nuclear superoxide promotes redistribution of these snoRNAs into the cytosol. Together, these data suggest the nucleocytoplasmic trafficking of snoRNAs is highly regulated. Moreover, the presence of snoRNAs in the cytosol provides a new context in which these snoRNAs may function in potentially novel roles beyond the modifications of rRNAs and snRNAs.

5.3 NXF3 as a snoRNA transporter

NXF family members have been identified based on sequence similarity and domain architecture that for most includes an amino terminal containing RNA binding domain (RBD), a p15/NXT-heterodimerization domain, and a carboxyl terminal domain involved in nuclear pore binding [102,103]. The RBD is conserved within the NXF family, however it is poorly defined for NXF3 as the predicted RBD does not bind to RNA, while the corresponding domains in NXF1 and NXF2 are capable of binding RNA [104,105]. The NXF family name implies that these proteins are primarily involved in nuclear export. Similar to NXF1, NXF3 is capable of associating with mRNA [67,73]. Prior studies in which RNA/protein complexes were isolated in cells transfected with an HA-tagged form of NXF3 using oligo dT cellulose. The complexes indicated a specific interaction between poly(A) RNA and HA-NXF3, providing evidence for a role of NXF3 in nuclear export of mRNA. Furthermore, a leucine-rich NES was identified within NXF3 that recruits CRM1 for its nuclear export activity [73].

Our data support a model in which NXF3 also has a role in importing RNAs to the nucleus. Knockdown of NXF3 resulted in an increase of cytosolic *Rpl13a* snoRNAs while overexpression resulted in a decrease. This data implicated NXF3 as a nuclear importer, efficiently returning snoRNAs from the cytosol to the nucleus under basal conditions. On the other hand, knockdown and overexpression of a related family member, NXF1, did not alter localization of the *Rpl13a* snoRNAs. Our study is the first to explore the potential contribution of NXF family members to snoRNA trafficking.

Together, our data suggest a new role specific to NXF3 as a nuclear importer for snoRNAs.

In both gain- and loss-of-function studies and in snoRNA binding studies, we compared NXF3 to NXF1. Although the effects of genetic manipulation on snoRNA localization were specific for NXF3, both family members are capable of binding the snoRNAs in co-immunoprecipitations. Although the RNA binding domains of NXF3 are not well characterized, NXF1 contains three RNA binding domains: RNA recognition motif (RRM), leucine-rich repeat, and NTF2-like domain [70]. The RRM has non-specific RNA binding activity [105]. It is possible that under the conditions of our immunoprecipitations, the RRM is capable of binding snoRNAs, even if this family member does not alter snoRNA distribution *in situ*. Future structure-function studies of NXF3 that target RNA binding requirements will provide important insights into this proteins role in snoRNA trafficking. It will also be of interest to compare NXF3 function in snoRNA trafficking to NXF family members in addition to NXF1

Some RNA export receptors directly bind to uncapped RNA targets, like miRNA and tRNA, while others require adaptor proteins like the cab binding complex (CBC) to bind to the caps of their target RNA, such as snRNA and mRNA [67]. Intiguingly, the snRNA export receptors CRM1 and PHAX are required for the intranuclear transport of independently transcribed, capped snoRNAs [75]. Whether CRM1 and PHAX function coordinately with NXF3 in snoRNA binding and movement between the nucleus and cytoplasm will be the subject of future studies.

While our data suggests that NXF3 regulates the localization of snoRNAs, the most direct way to demonstrate NXF3 acts as a snoRNA importer is to perform a nuclear import assay. However, this method has previously been established for proteins, not snoRNAs. We are currently developing a method with biotin-labeled snoRNAs and digitonin-permeablized cells. If successful, this method could also be extended to live-cell imaging and determine the kinetics of snoRNA transport under different conditions, like FSK treatment.

5.4 Regulation of NXF3-mediated snoRNA transport

To probe the regulation of snoRNA transport, we treated cells with adenylyl cyclase activator FSK to increase intracellular levels of cyclic AMP. FSK treatment depleted cytosolic snoRNAs, an effect that is dependent on NXF3. The increase in NXF3-snoRNA association and increase in nuclear localization of NXF3 suggested that the NXF3 import of snoRNAs is activated by FSK. On the other hand, DOX treatment increased cytosolic snoRNAs, decreased NXF3-snoRNA association and decreased nuclear localization of NXF3. However, the DOX effect was not dependent on NXF3. Together, our data suggest a model in which NXF3 plays a critical role in the return of snoRNAs from the cytoplasm to the nucleus, a pathway activated by FSK, but does not participate in DOX-stimulated snoRNA export.

FSK activates cyclic AMP signaling through both PKA-dependent and PKA-independent mechanisms [98-101]. This could lead to altered post-translational modifications, such as

phosphorylation of NXF3 or other proteins which function in snoRNA transport. Although examination of the NXF3 primary sequence suggests a number of potential phosphorylation sites, FSK did not change NXF3 phosphorylation, as determined using a panel of α-phospho-tyrosine, α-phospho-serine, and α-phospho-threonine antibodies. It is possible that the available antibodies lack appropriate specificity or that NXF3 is not a direct target of FSK. Structure function and proteomics studies will be necessary to address these possibilities. Furthermore, it is likely that NXF3 is acting in a complex of proteins similar to other RNA transport pathways and may be associated with another protein is phosphylated in response to FSK. In the future, immunoprecipitations could be coupled to mass spectrometry analyses to identify potential NXF3 protein partners. To confirm NXF3 transport is regulated by cyclic AMP, other inducers of intracellular levels of cyclic AMP like cholera toxin, phosphodiesterase inhibitors, or PKA inhibitors could be used [106]. Additionally, since FSK can activate cyclic AMP signaling through PKA-independent mechanisms, treating cells with PKA inhibitors could help narrow down the mechanism regulating NXF3 transport.

Our data have shown that the snoRNAs interact with NXF1 as well as NXF3. Given that knockdown and overexpression of NXF1 Does not affect cytosolic snoRNA levels, it will be of interest to test whether NXF1 association with the *Rpl13a* snoRNAs changes after FSK or DOX treatment, similar to NXF3. A finding that NXF1-snoRNA association is unchanged by FSK or that NXF1 knockdown has no effect on FSK-induced decreases in cytosolic snoRNAs, would provide further evidence of specificity for NXF3 function in snoRNA transport.

5.5 NXF3 and lipotoxicity

The physiological role of NXF3 is unclear. NXF3 has previously been shown to be dispensable for spermatogenesis, but its role in metabolic stress has not been investigated [107]. It would be interesting to develop a NXF3 knockdown mouse model and determine whether tissues are protected from metabolic stress such as lipid overload. Localization of snoRNAs could be measured from tissues isolated from this mouse model to confirm that loss of NXF3 alters snoRNA localization

Knockdown of NXF3 confers resistance to lipotoxicity, a process dependent on snoRNAs from the *Rpl13a* locus. Loss of NXF3 also alters distribution of these snoRNAs at baseline and prevents acute increase in cytosolic levels with lipotoxicity. The abundance of cytoplasmic *Rpl13a* snoRNAs in NXF3-knockdown cells is comparable to the levels achieved in control cells following acute lipotoxic exposure. This suggests that the dynamic change in cytosolic snoRNAs, rather than the absolute cytoplasmic levels of these non-coding RNAs is a key contributor to lipotoxic injury.

The role of cytosolic snoRNAs is still unknown. *Rpl13a* snoRNA knockdown cells had no change in methylation of their predicted rRNA targets, therefore suggesting a noncanonical targets for the *Rpl13a* snoRNAs. *In situ* hybridization studies revealed the *Rpl13a* snoRNAs localized in puncta in the cytosol after metabolic stress (CITE MICHEL 2011). It is possible that the snoRNAs are transported to specific organelles from the nucleus by NXF3. Future experiments should focus on determination of the

precise distribution and itinerary of snoRNAs once they leave the nucleus. Identifying the cytosolic localization could provide insight in the role of snoRNAs outside of the nucleus. A complete understanding of this new snoRNA biology requires further dissection of snoRNA trafficking and its regulation. Our identification of a role for NXF3 in regulated snoRNA trafficking represents a first step in this important direction.

CHAPTER SIX:
Materials and Methods

Materials—Digitonin, forskolin (FSK), phenylmethanesulfonyl fluoride (PMSF), cOmplete protease inhibitor cocktail, and hydrogen peroxide (H_2O_2) were from Sigma. Protein A Dynabeads, TURBO DNAse, and dihydroethidium (DHE) were from Thermo Fisher Scientific. Doxorubicin (DOX) was from Cayman Chemical. TRIzol LS and SUPERase-IN RNAse inhibitor was from Life Technologies. Dithiothreitol (DTT) was from CalBiochem and β-mercaptoethanol (BME) from Sigma. Laemmli Sample Buffer was from Bio-Rad.

Cells—H9c2 cardiomyoblasts and NIH3T3 fibroblasts were from American Type Culture Collection. Telomerase-immortalized human umbilical vein endothelial cells (HUVECs) were a gift from Judah Folkman's laboratory (Harvard Medical School) [108] H9c2 and 3T3 cells were maintained in Dulbecco's modified Eagle's medium (DMEM) with 10% heat inactivated fetal bovine serum (H9c2) or 10% calf serum (NIH3T3). HUVECs were maintained in endothelial cell growth medium (Lonza). DOX (20 μM for 1 h), FSK (10 μM for 1h), or H_2O_2 (1 mM, 4h) were added to media as indicated. Cell viability was determined using CellTiter-Glo Luminescent Cell Viability Assay (Promega). Basal cellular ROS was detected by staining cells (100,000 cells per well of 12-well dishes) with 10 μM DHE and detection using a microplate fluorescence reader (Tecan). Cells were transfected with plasmid DNA peGFP-1 (Clontech) and NXF3-GFP (gift from the Sun lab) [109] using Lipofectamine 2000 (Life Technologies) and with siRNAs (Life Technologies Silencer Select) using RNAiMax (Life Technologies), according to the

manufacturers' protocols. Flow cytometric analysis of transfected cells assessed fluorescence on 10^4 cells/sample.

shRNA screen—The shRNA screen was performed using a Decode Human GIPZ Lentiviral shRNAmir Library (Thermo Scientific). Immortalized HUVECs were transduced with lentiviral shRNA pools at MOI 0.1 then selected using puromycin. Puromycin-resistant cells were then treated with 500 μM palmitate for 48 h. After removing palmitate, cells were grown to form colonies in standard media. Colonies were hand-picked and re-tested for viability following lipotoxic exposure. For this, cells were plated in 96-well plate in triplicates (1000 cells per well) and treated with 500 μM palmitate for 24h. Cells transduced with non-targeting shRNA viral particles were used as negative control. Colonies with significantly greater viability than control cells were selected for further analysis. Genomic DNA was isolated from palmitate-resistant cells, and PCR was used to amplify barcodes corresponding to specific shRNAs for sequencing. Sequences were compared to the Decode shRNA libraries or analyzed using BLAST to identify the knocked down genes.

Subcellular Fractionation—For fractionation by detergent extraction, cell pellets were incubated in digitonin buffer (150mM NaCl, 50mM HEPES pH 7.4, digitonin 100μg/mL, EDTA 5mM, and SUPERase-In RNase inhibitor 0.1U/μL) for 10 min and centrifuged for 10 min at 2000g to yield a cytoplasmic supernatant and non-cytoplasmic pellet containing membranes and nuclei [110].

RNA isolation and quantitative real-time PCR—Total RNA was isolated from cytoplasmic or non-cytoplasmic fractions and from immunoprecipitates using TRIzol LS according to manufacturer's protocol (Life Technologies). cDNA was synthesized with SuperScript III First-strand Synthesis System (Invitrogen) using oligo-dT priming for mRNAs and target-specific stem-loop priming snoRNAs [45]. qPCR was performed using PerfeCTa SYBR Green SuperMix (Quantabio). Relative quantitation of target transcript expression was calculated using the ddCT method using Rplp0 as an endogenous control on an ABI 7500 Fast Real-time PCR system.

Immunoprecipitation—Cells were sonicated in 50 mM Tris pH 8.0, 150 mM NaCl, 2 mM EDTA, 0.5% NP40 containing 1X cOmplete protease inhibitor cocktail, 1 mM PMSF, and 0.1U/µl RNase inhibitor SUPERase-In. After treatment with 0.3U/µl TURBO DNase, insoluble material was removed by centrifugation at 20,000 x g for 10 min at 4°C. Lysate was incubated with α-GFP (2.5mg/mL) and Protein A Dynabeads for 4 h at 4°C. Complexes were washed four times with lysis buffer. Protein was eluted by incubation in 2X Laemmli Sample Buffer for western analysis, and RNA was eluted by incubation in TRIzol LS.

RNA sequencing—For cytosolic snoRNA sequencing experiments, H9c2 cells from 3 independent experiments were treated as indicated, cytosol was recovered by detergent extraction, and total RNA was isolated using TRIzol LS followed by Qiagen RNeasy miRNA clean up. Input and immunoprecipitated RNA from 3T3 cells from 3 independent experiments was isolated and concentrated using RNA Clean & Concentrator-5 (Zymo

Research). Indexed RNA-sequencing libraries were made using the Illumina TruSeq small RNA kit. Libraries were amplified with 14 cycles of PCR, pooled, and separated by PAGE. Products with sizes 30-375 nucleotides were excised and collected from the gel. Sequencing was performed using an Illumina HiSeq 2500. Demultiplexed data were analyzed using Partek Flow (build version 6.0.17.0305 Copyright ©; 2017 Partek Inc., St. Louis, MO, USA). H9c2 sequences were uploaded to Galaxy. Sequences were evaluated for quality by FASTQC, trimming was applied to reject scores of <20, and sequences were clipped to remove adapter sequence. Sequences were aligned to the rat genome (rn4, Bowtie for Illumina, default settings) and aligned reads were exported to Partek Genomics Suite (v.6.6) for annotation and quantitative analysis using the rat genome build that contains snoRNAs (Ensembl Build e69, RGSC3.4.69).

For NXF3 pulldown studies in NIH 3T3 cells, sequences were evaluated for quality and trimmed to remove adapter sequence. A custom Linux script was used to remove murine ribosomal sequences according to the Illumina iGenome murine genome annotation. Remaining sequences were aligned to the murine genome (mm9 Refseq Transcript 2016-08-01, Bowtie for Illumina, default settings) and aligned reads were quantified, normalized and annotated. Analysis was limited to genes with >100 aligned reads. A step-up FDR of 0.05 was considered significant.

Immunoblots—Protein in total, cytoplasmic and non-cytoplasmic fractions was quantified by bicinchoninic assay (BCA, Thermo Fisher Scientific), separated by SDS-PAGE, and immunoblotted. Detection for human nuclear export factor 3 (NXF3; Abcam ab76430, 1:500), GFP (Abcam ab290, 1:5000), heat shock protein 90 (HSP90; Enzo

SPA-846, 1:1000), α-tubulin (α-TUB; Sigma T6199, 1:2000), histone H3 (H3; Abcam ab1791, 1:5000), and nucleophosmin (NPM; Abcam ab37659, 1:1500) used horseradish peroxidase-conjugated secondary antibodies (Jackson Immuno Research Laboratories) and Western Lightning Plus-ECL (Perkin Elmer) using a ChemiDoc Imaging System.

Immunofluorescence—Cells were grown on glass coverslips coated with 0.8% gelatin, fixed with 4% paraformaldehyde, permeabilized with NP40, and blocked with 200μg/mL ChromPure IgG (Jackson Immuno Research Laboratories) corresponding to secondary antibody species. Detection for NPM used α-NPM (Life Technologies 325200; 1:1000) with secondary Alexa Fluor 350 donkey anti-mouse IgG (Life Technologies A10035; 40μg/mL). GFP transfected cells were grown on glass coverslips and fixed with 4% paraformaldehyde. Coverslips were mounted on microscope slides using SlowFade Antifade reagent (Life Technologies S2828). Slides were imaged on a Zeiss Axioskop 2 mot plus microscope with a Zeiss AxioCam MRm camera with a x40 oil immersion objective at room temperature. Images were acquired using AxioVision Rel. 4.8 software. Images were processed identically using the ImageJ software package (rsb.info.nih.gov).

Statistics—Biochemical results are presented as mean + SEM for a minimum of 3 independent experiments. Statistical significance was assessed by two-tailed unpaired t-test. P-value < 0.05 was considered significant.

CHAPTER SEVEN:
References

1 Morrish, N. J., Wang, S. L., Stevens, L. K., Fuller, J. H. & Keen, H. Mortality and causes of death in the WHO Multinational Study of Vascular Disease in Diabetes. *Diabetologia* **44 Suppl 2**, S14-21 (2001).

2 Fonarow, G. C. & Srikanthan, P. Diabetic cardiomyopathy. *Endocrinology and metabolism clinics of North America* **35**, 575-599, ix, doi:10.1016/j.ecl.2006.05.003 (2006).

3 Voulgari, C., Papadogiannis, D. & Tentolouris, N. Diabetic cardiomyopathy: from the pathophysiology of the cardiac myocytes to current diagnosis and management strategies. *Vascular health and risk management* **6**, 883-903, doi:10.2147/VHRM.S11681 (2010).

4 Beckman, J. A., Creager, M. A. & Libby, P. Diabetes and atherosclerosis: epidemiology, pathophysiology, and management. *Jama* **287**, 2570-2581 (2002).

5 Giovannucci, E. *et al.* Diabetes and cancer: a consensus report. *Diabetes care* **33**, 1674-1685, doi:10.2337/dc10-0666 (2010).

6 Bommer, C. *et al.* The global economic burden of diabetes in adults aged 20-79 years: a cost-of-illness study. *The lancet. Diabetes & endocrinology* **5**, 423-430, doi:10.1016/S2213-8587(17)30097-9 (2017).

7 Daneman, D. Type 1 diabetes. *Lancet* **367**, 847-858, doi:10.1016/S0140-6736(06)68341-4 (2006).

8 Bornfeldt, K. E. & Tabas, I. Insulin resistance, hyperglycemia, and atherosclerosis. *Cell metabolism* **14**, 575-585, doi:10.1016/j.cmet.2011.07.015 (2011).

9 Rahman, S., Rahman, T., Ismail, A. A. & Rashid, A. R. Diabetes-associated macrovasculopathy: pathophysiology and pathogenesis. *Diabetes, obesity & metabolism* **9**, 767-780, doi:10.1111/j.1463-1326.2006.00655.x (2007).

10 Giacco, F. & Brownlee, M. Oxidative stress and diabetic complications. *Circulation research* **107**, 1058-1070, doi:10.1161/CIRCRESAHA.110.223545 (2010).

11 Campos, C. Chronic hyperglycemia and glucose toxicity: pathology and clinical sequelae. *Postgraduate medicine* **124**, 90-97, doi:10.3810/pgm.2012.11.2615 (2012).

12 Nathan, D. M. *et al.* Intensive diabetes treatment and cardiovascular disease in patients with type 1 diabetes. *The New England journal of medicine* **353**, 2643-2653, doi:10.1056/NEJMoa052187 (2005).

13 Action to Control Cardiovascular Risk in Diabetes Study, G. *et al.* Effects of intensive glucose lowering in type 2 diabetes. *The New England journal of medicine* **358**, 2545-2559, doi:10.1056/NEJMoa0802743 (2008).

14 Haffner, S. M. Management of dyslipidemia in adults with diabetes. *Diabetes care* **21**, 160-178 (1998).

15 Howard, B. V. Lipoprotein metabolism in diabetes mellitus. *Journal of lipid research* **28**, 613-628 (1987).

16 Lewis, G. F., Carpentier, A., Adeli, K. & Giacca, A. Disordered fat storage and mobilization in the pathogenesis of insulin resistance and type 2 diabetes. *Endocrine reviews* **23**, 201-229, doi:10.1210/edrv.23.2.0461 (2002).

17 Wiggin, T. D. *et al.* Elevated triglycerides correlate with progression of diabetic neuropathy. *Diabetes* **58**, 1634-1640, doi:10.2337/db08-1771 (2009).

18 Miljanovic, B., Glynn, R. J., Nathan, D. M., Manson, J. E. & Schaumberg, D. A. A prospective study of serum lipids and risk of diabetic macular edema in type 1 diabetes. *Diabetes* **53**, 2883-2892 (2004).

19 Kashyap, S. R. *et al.* Triglyceride levels and not adipokine concentrations are closely related to severity of nonalcoholic fatty liver disease in an obesity surgery cohort. *Obesity* **17**, 1696-1701, doi:10.1038/oby.2009.89 (2009).

20 Ebong, I. A. *et al.* Association of lipids with incident heart failure among adults with and without diabetes mellitus: Multiethnic Study of Atherosclerosis. *Circulation. Heart failure* **6**, 371-378, doi:10.1161/CIRCHEARTFAILURE.112.000093 (2013).

21 Ameer, F., Scandiuzzi, L., Hasnain, S., Kalbacher, H. & Zaidi, N. De novo lipogenesis in health and disease. *Metabolism: clinical and experimental* **63**, 895-902, doi:10.1016/j.metabol.2014.04.003 (2014).

22 Griffin, M. E. *et al.* Free fatty acid-induced insulin resistance is associated with activation of protein kinase C theta and alterations in the insulin signaling cascade. *Diabetes* **48**, 1270-1274 (1999).

23 Martins, A. R. *et al.* Mechanisms underlying skeletal muscle insulin resistance induced by fatty acids: importance of the mitochondrial function. *Lipids in health and disease* **11**, 30, doi:10.1186/1476-511X-11-30 (2012).

24 Yu, C. *et al.* Mechanism by which fatty acids inhibit insulin activation of insulin receptor substrate-1 (IRS-1)-associated phosphatidylinositol 3-kinase activity in

muscle. *The Journal of biological chemistry* **277**, 50230-50236, doi:10.1074/jbc.M200958200 (2002).

25 Kuramoto, K. *et al.* Perilipin 5, a lipid droplet-binding protein, protects heart from oxidative burden by sequestering fatty acid from excessive oxidation. *The Journal of biological chemistry* **287**, 23852-23863, doi:10.1074/jbc.M111.328708 (2012).

26 Listenberger, L. L. *et al.* Triglyceride accumulation protects against fatty acid-induced lipotoxicity. *Proceedings of the National Academy of Sciences of the United States of America* **100**, 3077-3082, doi:10.1073/pnas.0630588100 (2003).

27 Liu, L. *et al.* DGAT1 expression increases heart triglyceride content but ameliorates lipotoxicity. *The Journal of biological chemistry* **284**, 36312-36323, doi:10.1074/jbc.M109.049817 (2009).

28 Zheng, P. *et al.* Plin5 alleviates myocardial ischaemia/reperfusion injury by reducing oxidative stress through inhibiting the lipolysis of lipid droplets. *Scientific reports* **7**, 42574, doi:10.1038/srep42574 (2017).

29 Preiser, J. C. Oxidative stress. *JPEN. Journal of parenteral and enteral nutrition* **36**, 147-154, doi:10.1177/0148607111434963 (2012).

30 Touyz, R. M., Briones, A. M., Sedeek, M., Burger, D. & Montezano, A. C. NOX isoforms and reactive oxygen species in vascular health. *Molecular interventions* **11**, 27-35, doi:10.1124/mi.11.1.5 (2011).

31 Borradaile, N. M. *et al.* Disruption of endoplasmic reticulum structure and integrity in lipotoxic cell death. *Journal of lipid research* **47**, 2726-2737, doi:10.1194/jlr.M600299-JLR200 (2006).

32 Inoguchi, T. *et al.* High glucose level and free fatty acid stimulate reactive oxygen species production through protein kinase C--dependent activation of NAD(P)H oxidase in cultured vascular cells. *Diabetes* **49**, 1939-1945 (2000).

33 Kharroubi, I. *et al.* Free fatty acids and cytokines induce pancreatic beta-cell apoptosis by different mechanisms: role of nuclear factor-kappaB and endoplasmic reticulum stress. *Endocrinology* **145**, 5087-5096, doi:10.1210/en.2004-0478 (2004).

34 Ostrander, D. B., Sparagna, G. C., Amoscato, A. A., McMillin, J. B. & Dowhan, W. Decreased cardiolipin synthesis corresponds with cytochrome c release in palmitate-induced cardiomyocyte apoptosis. *The Journal of biological chemistry* **276**, 38061-38067, doi:10.1074/jbc.M107067200 (2001).

35 Schroder, M. & Kaufman, R. J. ER stress and the unfolded protein response. *Mutation research* **569**, 29-63, doi:10.1016/j.mrfmmm.2004.06.056 (2005).

36 Han, J. & Kaufman, R. J. The role of ER stress in lipid metabolism and lipotoxicity. *Journal of lipid research* **57**, 1329-1338, doi:10.1194/jlr.R067595 (2016).

37 Ceriello, A. & Motz, E. Is oxidative stress the pathogenic mechanism underlying insulin resistance, diabetes, and cardiovascular disease? The common soil hypothesis revisited. *Arteriosclerosis, thrombosis, and vascular biology* **24**, 816-823, doi:10.1161/01.ATV.0000122852.22604.78 (2004).

38 Listenberger, L. L., Ory, D. S. & Schaffer, J. E. Palmitate-induced apoptosis can occur through a ceramide-independent pathway. *The Journal of biological chemistry* **276**, 14890-14895, doi:10.1074/jbc.M010286200 (2001).

39 Browning, J. D. & Horton, J. D. Molecular mediators of hepatic steatosis and liver injury. *The Journal of clinical investigation* **114**, 147-152, doi:10.1172/JCI22422 (2004).

40 de Vries, A. P. *et al.* Fatty kidney: emerging role of ectopic lipid in obesity-related renal disease. *The lancet. Diabetes & endocrinology* **2**, 417-426, doi:10.1016/S2213-8587(14)70065-8 (2014).

41 Goldberg, I. J., Trent, C. M. & Schulze, P. C. Lipid metabolism and toxicity in the heart. *Cell metabolism* **15**, 805-812, doi:10.1016/j.cmet.2012.04.006 (2012).

42 Garg, A. Clinical review#: Lipodystrophies: genetic and acquired body fat disorders. *The Journal of clinical endocrinology and metabolism* **96**, 3313-3325, doi:10.1210/jc.2011-1159 (2011).

43 Brookheart, R. T., Michel, C. I. & Schaffer, J. E. As a matter of fat. *Cell metabolism* **10**, 9-12, doi:10.1016/j.cmet.2009.03.011 (2009).

44 Caputa, G. *et al.* RNASET2 is required for ROS propagation during oxidative stress-mediated cell death. *Cell death and differentiation* **23**, 347-357, doi:10.1038/cdd.2015.105 (2016).

45 Michel, C. I. *et al.* Small nucleolar RNAs U32a, U33, and U35a are critical mediators of metabolic stress. *Cell metabolism* **14**, 33-44, doi:10.1016/j.cmet.2011.04.009 (2011).

46 Scruggs, B. S., Michel, C. I., Ory, D. S. & Schaffer, J. E. SmD3 regulates intronic noncoding RNA biogenesis. *Molecular and cellular biology* **32**, 4092-4103, doi:10.1128/MCB.00022-12 (2012).

47 Holley, C. L. *et al.* Cytosolic accumulation of small nucleolar RNAs (snoRNAs) is dynamically regulated by NADPH oxidase. *The Journal of biological chemistry* **290**, 11741-11748, doi:10.1074/jbc.M115.637413 (2015).

48 Speckmann, W. A., Terns, R. M. & Terns, M. P. The box C/D motif directs snoRNA 5'-cap hypermethylation. *Nucleic acids research* **28**, 4467-4473 (2000).

49 Darzacq, X. *et al.* Cajal body-specific small nuclear RNAs: a novel class of 2'-O-methylation and pseudouridylation guide RNAs. *The EMBO journal* **21**, 2746-2756, doi:10.1093/emboj/21.11.2746 (2002).

50 Bazeley, P. S. *et al.* snoTARGET shows that human orphan snoRNA targets locate close to alternative splice junctions. *Gene* **408**, 172-179, doi:10.1016/j.gene.2007.10.037 (2008).

51 Filipowicz, W. & Pogacic, V. Biogenesis of small nucleolar ribonucleoproteins. *Current opinion in cell biology* **14**, 319-327 (2002).

52 Kiss, T. Small nucleolar RNA-guided post-transcriptional modification of cellular RNAs. *The EMBO journal* **20**, 3617-3622, doi:10.1093/emboj/20.14.3617 (2001).

53 Tycowski, K. T., You, Z. H., Graham, P. J. & Steitz, J. A. Modification of U6 spliceosomal RNA is guided by other small RNAs. *Molecular cell* **2**, 629-638 (1998).

54 Weinstein, L. B. & Steitz, J. A. Guided tours: from precursor snoRNA to functional snoRNP. *Current opinion in cell biology* **11**, 378-384, doi:10.1016/S0955-0674(99)80053-2 (1999).

55 Dragon, F. *et al.* A large nucleolar U3 ribonucleoprotein required for 18S ribosomal RNA biogenesis. *Nature* **417**, 967-970, doi:10.1038/nature00769 (2002).

56 King, T. H., Liu, B., McCully, R. R. & Fournier, M. J. Ribosome structure and activity are altered in cells lacking snoRNPs that form pseudouridines in the peptidyl transferase center. *Molecular cell* **11**, 425-435 (2003).

57 Kishore, S. *et al.* The snoRNA MBII-52 (SNORD 115) is processed into smaller RNAs and regulates alternative splicing. *Human molecular genetics* **19**, 1153-1164, doi:10.1093/hmg/ddp585 (2010).

58 Vitali, P. *et al.* ADAR2-mediated editing of RNA substrates in the nucleolus is inhibited by C/D small nucleolar RNAs. *The Journal of cell biology* **169**, 745-753, doi:10.1083/jcb.200411129 (2005).

59 Ender, C. *et al.* A human snoRNA with microRNA-like functions. *Molecular cell* **32**, 519-528, doi:10.1016/j.molcel.2008.10.017 (2008).

60 Schwartz, S. *et al.* Transcriptome-wide mapping reveals widespread dynamic-regulated pseudouridylation of ncRNA and mRNA. *Cell* **159**, 148-162, doi:10.1016/j.cell.2014.08.028 (2014).

61 Lee, J. *et al.* Rpl13a small nucleolar RNAs regulate systemic glucose metabolism. *The Journal of clinical investigation* **126**, 4616-4625, doi:10.1172/JCI88069 (2016).

62 Siprashvili, Z. *et al.* The noncoding RNAs SNORD50A and SNORD50B bind K-Ras and are recurrently deleted in human cancer. *Nature genetics* **48**, 53-58, doi:10.1038/ng.3452 (2016).

63 Mei, Y. P. *et al.* Small nucleolar RNA 42 acts as an oncogene in lung tumorigenesis. *Oncogene* **31**, 2794-2804, doi:10.1038/onc.2011.449 (2012).

64 Zhou, F. *et al.* AML1-ETO requires enhanced C/D box snoRNA/RNP formation to induce self-renewal and leukaemia. *Nature cell biology* **19**, 844-855, doi:10.1038/ncb3563 (2017).

65 Herold, A., Klymenko, T. & Izaurralde, E. NXF1/p15 heterodimers are essential for mRNA nuclear export in Drosophila. *Rna* **7**, 1768-1780 (2001).

66 Suyama, M. *et al.* Prediction of structural domains of TAP reveals details of its interaction with p15 and nucleoporins. *EMBO reports* **1**, 53-58, doi:10.1038/sj.embor.embor627 (2000).

67 Kohler, A. & Hurt, E. Exporting RNA from the nucleus to the cytoplasm. *Nature reviews. Molecular cell biology* **8**, 761-773, doi:10.1038/nrm2255 (2007).

68 Jun, L. *et al.* NXF5, a novel member of the nuclear RNA export factor family, is lost in a male patient with a syndromic form of mental retardation. *Current biology : CB* **11**, 1381-1391 (2001).

69 Kang, Y. & Cullen, B. R. The human Tap protein is a nuclear mRNA export factor that contains novel RNA-binding and nucleocytoplasmic transport sequences. *Genes & development* **13**, 1126-1139 (1999).

70 Katahira, J., Dimitrova, L., Imai, Y. & Hurt, E. NTF2-like domain of Tap plays a critical role in cargo mRNA recognition and export. *Nucleic acids research* **43**, 1894-1904, doi:10.1093/nar/gkv039 (2015).

71 Kuersten, S., Segal, S. P., Verheyden, J., LaMartina, S. M. & Goodwin, E. B. NXF-2, REF-1, and REF-2 affect the choice of nuclear export pathway for tra-2 mRNA in C. elegans. *Molecular cell* **14**, 599-610, doi:10.1016/j.molcel.2004.05.004 (2004).

72 Tretyakova, I. *et al.* Nuclear export factor family protein participates in cytoplasmic mRNA trafficking. *The Journal of biological chemistry* **280**, 31981-31990, doi:10.1074/jbc.M502736200 (2005).

73 Yang, J., Bogerd, H. P., Wang, P. J., Page, D. C. & Cullen, B. R. Two closely related human nuclear export factors utilize entirely distinct export pathways. *Molecular cell* **8**, 397-406 (2001).

74 Falaleeva, M. & Stamm, S. Processing of snoRNAs as a new source of regulatory non-coding RNAs: snoRNA fragments form a new class of functional RNAs. *BioEssays : news and reviews in molecular, cellular and developmental biology* **35**, 46-54, doi:10.1002/bies.201200117 (2013).

75 Boulon, S. *et al.* PHAX and CRM1 are required sequentially to transport U3 snoRNA to nucleoli. *Molecular cell* **16**, 777-787, doi:10.1016/j.molcel.2004.11.013 (2004).

76 Watkins, N. J., Lemm, I. & Luhrmann, R. Involvement of nuclear import and export factors in U8 box C/D snoRNP biogenesis. *Molecular and cellular biology* **27**, 7018-7027, doi:10.1128/MCB.00516-07 (2007).

77 Lenaz, G. The mitochondrial production of reactive oxygen species: mechanisms and implications in human pathology. *IUBMB life* **52**, 159-164, doi:10.1080/15216540152845957 (2001).

78 Nordberg, J. & Arner, E. S. Reactive oxygen species, antioxidants, and the mammalian thioredoxin system. *Free radical biology & medicine* **31**, 1287-1312 (2001).

79 Ushio-Fukai, M., Zafari, A. M., Fukui, T., Ishizaka, N. & Griendling, K. K. p22phox is a critical component of the superoxide-generating NADH/NADPH oxidase system and regulates angiotensin II-induced hypertrophy in vascular smooth muscle cells. *The Journal of biological chemistry* **271**, 23317-23321 (1996).

80 Kuroda, J. *et al.* NADPH oxidase 4 (Nox4) is a major source of oxidative stress in the failing heart. *Proceedings of the National Academy of Sciences of the United States of America* **107**, 15565-15570, doi:10.1073/pnas.1002178107 (2010).

81 Goyal, P. *et al.* Identification of novel Nox4 splice variants with impact on ROS levels in A549 cells. *Biochemical and biophysical research communications* **329**, 32-39, doi:10.1016/j.bbrc.2005.01.089 (2005).

82 Anilkumar, N. *et al.* A 28-kDa splice variant of NADPH oxidase-4 is nuclear-localized and involved in redox signaling in vascular cells. *Arteriosclerosis, thrombosis, and vascular biology* **33**, e104-112, doi:10.1161/ATVBAHA.112.300956 (2013).

83 Wang, S. *et al.* Doxorubicin induces apoptosis in normal and tumor cells via distinctly different mechanisms. intermediacy of H(2)O(2)- and p53-dependent pathways. *The Journal of biological chemistry* **279**, 25535-25543, doi:10.1074/jbc.M400944200 (2004).

84 Deng, S. *et al.* Gp91phox-containing NAD(P)H oxidase increases superoxide formation by doxorubicin and NADPH. *Free radical biology & medicine* **42**, 466-473, doi:10.1016/j.freeradbiomed.2006.11.013 (2007).

85 Gilleron, M. *et al.* NADPH oxidases participate to doxorubicin-induced cardiac myocyte apoptosis. *Biochemical and biophysical research communications* **388**, 727-731, doi:10.1016/j.bbrc.2009.08.085 (2009).

86 Li, J. Z., Yu, S. Y., Wu, J. H., Shao, Q. R. & Dong, X. M. Paeoniflorin protects myocardial cell from doxorubicin-induced apoptosis through inhibition of NADPH oxidase. *Canadian journal of physiology and pharmacology* **90**, 1569-1575, doi:10.1139/y2012-140 (2012).

87 Yang, K. *et al.* A redox mechanism underlying nucleolar stress sensing by nucleophosmin. *Nature communications* **7**, 13599, doi:10.1038/ncomms13599 (2016).

88 Matsushima, S. *et al.* Increased oxidative stress in the nucleus caused by Nox4 mediates oxidation of HDAC4 and cardiac hypertrophy. *Circulation research* **112**, 651-663, doi:10.1161/CIRCRESAHA.112.279760 (2013).

89 Youssef, O. A. *et al.* Potential role for snoRNAs in PKR activation during metabolic stress. *Proceedings of the National Academy of Sciences of the United States of America* **112**, 5023-5028, doi:10.1073/pnas.1424044112 (2015).

90 Sienna, N., Larson, D. E. & Sells, B. H. Altered subcellular distribution of U3 snRNA in response to serum in mouse fibroblasts. *Experimental cell research* **227**, 98-105, doi:10.1006/excr.1996.0254 (1996).

91 Yang, J. *et al.* Control of cyclin B1 localization through regulated binding of the nuclear export factor CRM1. *Genes & development* **12**, 2131-2143 (1998).

92 Shanker, S. *et al.* Evaluation of commercially available RNA amplification kits for RNA sequencing using very low input amounts of total RNA. *Journal of biomolecular techniques : JBT* **26**, 4-18, doi:10.7171/jbt.15-2601-001 (2015).

93 Dupuis-Sandoval, F., Poirier, M. & Scott, M. S. The emerging landscape of small nucleolar RNAs in cell biology. *Wiley interdisciplinary reviews. RNA* **6**, 381-397, doi:10.1002/wrna.1284 (2015).

94 Fasold, M., Langenberger, D., Binder, H., Stadler, P. F. & Hoffmann, S. DARIO: a ncRNA detection and analysis tool for next-generation sequencing experiments. *Nucleic acids research* **39**, W112-117, doi:10.1093/nar/gkr357 (2011).

95 Lestrade, L. & Weber, M. J. snoRNA-LBME-db, a comprehensive database of human H/ACA and C/D box snoRNAs. *Nucleic acids research* **34**, D158-162, doi:10.1093/nar/gkj002 (2006).

96 Nigg, E. A. Nucleocytoplasmic transport: signals, mechanisms and regulation. *Nature* **386**, 779-787, doi:10.1038/386779a0 (1997).

97 Seamon, K. B. & Daly, J. W. Forskolin: a unique diterpene activator of cyclic AMP-generating systems. *Journal of cyclic nucleotide research* **7**, 201-224 (1981).

98 Delghandi, M. P., Johannessen, M. & Moens, U. The cAMP signalling pathway activates CREB through PKA, p38 and MSK1 in NIH 3T3 cells. *Cellular signalling* **17**, 1343-1351, doi:10.1016/j.cellsig.2005.02.003 (2005).

99 Galli, C. *et al.* Apoptosis in cerebellar granule cells is blocked by high KCl, forskolin, and IGF-1 through distinct mechanisms of action: the involvement of intracellular calcium and RNA synthesis. *The Journal of neuroscience : the official journal of the Society for Neuroscience* **15**, 1172-1179 (1995).

100 Hoque, K. M. *et al.* Epac1 mediates protein kinase A-independent mechanism of forskolin-activated intestinal chloride secretion. *The Journal of general physiology* **135**, 43-58, doi:10.1085/jgp.200910339 (2010).

101 Namkoong, S. *et al.* Forskolin increases angiogenesis through the coordinated cross-talk of PKA-dependent VEGF expression and Epac-mediated PI3K/Akt/eNOS signaling. *Cellular signalling* **21**, 906-915 (2009).

102 Izaurralde, E. Friedrich Miescher Prize awardee lecture review. A conserved family of nuclear export receptors mediates the exit of messenger RNA to the cytoplasm. *Cellular and molecular life sciences : CMLS* **58**, 1105-1112, doi:10.1007/PL00000924 (2001).

103 Sasaki, M. *et al.* Molecular cloning and functional characterization of mouse Nxf family gene products. *Genomics* **85**, 641-653, doi:10.1016/j.ygeno.2005.01.003 (2005).

104 Herold, A. *et al.* TAP (NXF1) belongs to a multigene family of putative RNA export factors with a conserved modular architecture. *Molecular and cellular biology* **20**, 8996-9008 (2000).

105 Liker, E., Fernandez, E., Izaurralde, E. & Conti, E. The structure of the mRNA export factor TAP reveals a cis arrangement of a non-canonical RNP domain and an LRR domain. *The EMBO journal* **19**, 5587-5598, doi:10.1093/emboj/19.21.5587 (2000).

106 Yan, K., Gao, L. N., Cui, Y. L., Zhang, Y. & Zhou, X. The cyclic AMP signaling pathway: Exploring targets for successful drug discovery (Review). *Molecular medicine reports* **13**, 3715-3723, doi:10.3892/mmr.2016.5005 (2016).

107 Zhou, J. *et al.* Nxf3 is expressed in Sertoli cells, but is dispensable for spermatogenesis. *Molecular reproduction and development* **78**, 241-249, doi:10.1002/mrd.21291 (2011).

108 Freedman, D. A. & Folkman, J. Maintenance of G1 checkpoint controls in telomerase-immortalized endothelial cells. *Cell cycle* **3**, 811-816 (2004).

109 Yin, Y. *et al.* Nuclear export factor 3 is involved in regulating the expression of TGF-beta3 in an mRNA export activity-independent manner in mouse Sertoli cells. *The Biochemical journal* **452**, 67-78, doi:10.1042/BJ20121006 (2013).

110 Holden, P. & Horton, W. A. Crude subcellular fractionation of cultured mammalian cell lines. *BMC research notes* **2**, 243, doi:10.1186/1756-0500-2-243 (2009).